U-Th isotope constraints on gas hydrate and pockmark dynamics at the Niger delta margin

Bayon Germain [1, *], Henderson Gideon M. [2], Etoubleau Joel [1], Caprais Jean-Claude [3], Ruffine Livio [1], Marsset Tania [1], Dennielou Bernard [1], Cauquil Eric [4], Voisset Michel [1], Sultan Nabil [1]

[1] IFREMER, Unite Rech Geosci Marines, F-29280 Plouzane, France.
[2] Univ Oxford, Dept Earth Sci, Oxford OX1 3PR, England.
[3] IFREMER, Unite Rech Etud Ecosyst Profonds, F-29280 Plouzane, France.
[4] TOTAL, F-92069 Paris, France.

* Corresponding author, Germain Bayon, email address : gbayon@ifremer.fr

Abstract :

The application of uranium-thorium dating methods to authigenic carbonates provides unique constraints on the temporal evolution of methane seeps at ocean margins. In this study, we report U-Th isotope measurements for carbonate breccias collected from within a hydrate-bearing pockmark located at the Niger Delta margin. These concretions were extracted from a carbonate-rich layer in the upper two meters of a sediment core (N2-KS-44; ~ 1200 m water depth), well above the present-day sulphate-methane transition zone (about 3 m depth) and the presence of gas hydrates in the sediment. The stratigraphy of core N2-KS-44 was established by tuning its downcore Al/Ti profile to a well-dated nearby reference core, and carbonate 230Th/U ages were calculated using isochron methods.

Our results indicate that a major event of aragonite precipitation occurred between about 13 and 2.5 ka at the studied location. Comparison of sediment accumulation rates at both core N2-KS-44 and the nearby reference site suggests that the initial stage of carbonate precipitation, between 13 and 10 ka, was associated with sediment winnowing, probably related to intense fluid seepage. In contrast, our data indicate that sedimentation rates rapidly increased within the pockmark after 7 ka. In agreement with the presence of carbonate breccias exhibiting U-Th ages older than their corresponding stratigraphic age, this observation would suggest that sediment reworking took place after that time, possibly caused by erosion of the surrounding sediment within the pockmark. We hypothesize that the period of carbonate formation between 13 and 2.5 ka was related to an upward migration of gas-hydrate reservoirs to the near seafloor environment. After this pulse of enhanced fluid flow, the diminution of methane fluxes at the base of the local gas-hydrate occurrence zone would have led to hydrate dissolution in sub-surface sediments and pockmark formation, thereby explaining the progressive increase in sedimentation rates, the absence of recent carbonate concretions and the deepening of the sulphate-methane transition zone at site N2-KS-44 inferred from pore water data. Overall, these results provide further constraints about the relationship between gas hydrate dynamics and the evolution of pockmarks at ocean margins through time.

Highlights

► Breccias from hydrate-bearing sediments can be successfully dated with U-series. ► Seep carbonates precipitated between 13.0 and 2.5 kyr at the studied pockmark. ► Evidence for hydrate dissolution and SMTZ fluctuations during the Holocene. ► Co-evolution of gas hydrate and pockmark dynamics through time.

Keywords : Gas hydrates, Pockmarks, U-series, Authigenic carbonates, Niger delta

1. Introduction

Huge amounts of methane (CH_4) are stored as gas hydrates at ocean margins (Milkov, 2004; Wallmann et al., 2012), representing potentially an important component of the global carbon and methane cycles (Judd et al., 2002; Dickens, 2003). Gas hydrates are unstable phases in marine sediments, which may decompose in response to small changes in gas-saturation of the surrounding pore water, or to changes in the pressure and temperature conditions of the marine environment, such as those induced by sea-level changes, continental-slope failures, and the reorganisation of deep-ocean circulation or fluid pathway systems within the sediment column (Buffett, 2000). While isotopic records of atmospheric CH_4 in ice cores indicate negligible contribution from marine gas hydrate reservoirs during the Late Quaternary (Sowers, 2006), dissociation of gas hydrates stored at margins could have led episodically to substantial methane releases in the past, possibly affecting both the marine environment and the atmosphere (e.g. Nisbett, 1990; Haq, 1998; Kennett et al., 2000; Hesselbo et al., 2000; Bangs et al., 2010). At ocean margins, the occurrence of gas hydrates in near-seafloor sediments is often associated with the presence of pockmarks, which correspond to seabed depressions related to seepage of methane-rich fluids (Hovland and Judd, 1988; Suess, 2014). Over the past decades, there has been increasing evidence for widespread distribution of both active and inactive pockmarks at margins, which questions their relationship to past fluid seepage and potential episodes of gas hydrate dissociation (e.g. Hovland et al., 2002; Loncke et al., 2004; Davy et al., 2010; Sultan et al., 2010; Pau et al., 2014). While pockmarks are being increasingly studied, however, there are still significant uncertainties on the factors controlling their activity and their evolution through time. In particular, knowledge on both the timing and duration of pockmark activity is important for constraining the possible links between climate change and methane seeps in the past.

Evidence for past methane releases and gas hydrate destabilisation in marine sediments has come primarily from carbon isotope signals in geological records (e.g. Dickens et al., 1995; Kennett et al., 2000; Hesselbo et al., 2000; Hill et al., 2004; Panieri et al., 2014). Because methane stored in sedimentary gas hydrates exhibits highly

63   negative carbon isotope signatures, large negative $\delta^{13}C$ excursions recorded by

64   foraminifera in marine sediments have been interpreted as indicators for past circulation

65   of methane-rich fluids potentially related to the dissociation of methane hydrates (e.g.

66   Kennett et al., 2000; Smith et al., 2001; Panieri et al., 2014). Authigenic carbonates

67   represent another potential archive of past fluid flow and gas-hydrate dissociation on

68   continental margins (Bohrmann et al., 1998; Naehr et al., 2000; Greinert et al., 2001).

69   The occurrence of authigenic carbonate deposits (e.g. chemoherm carbonates, carbonate

70   crusts and nodules) has been reported at many seeps worldwide (Suess, 2014). Cold seep

71   carbonates result primarily from the microbial anaerobic oxidation of methane (AOM) in

72   sediments (Boetius et al., 2000), which typically leads to enhanced alkalinity levels in

73   surrounding pore waters and, as a consequence, to carbonate precipitation. In gas-

74   hydrate-bearing sediments, authigenic carbonates often occur as millimeter- to

75   centimeter-size nodules of carbonate-cemented mudclast breccias or nodules (Bohrmann

76   et al., 1998; Naehr et al., 2000; Greinert et al., 2001; Bayon et al., 2007). It has been

77   suggested that such carbonates represent suitable paleo-indicators for the presence of gas

78   hydrates in marine sediments (Naehr et al., 2000; Pierre et al., 2000; Bayon et al., 2007).

79

80   Absolute dating of authigenic carbonate breccias or nodules recovered at various

81   depths within hydrate-bearing sediments can thus provide unique constraints on past

82   methane fluxes, and the evolution of gas-hydrate reservoirs in marine sediments through

83   time. Conventional ^{14}C dating is usually not applicable to authigenic carbonates because

84   their carbon partly derives from old fossil sources (i.e. methane), but several studies have

85   now demonstrated that uranium-thorium dating techniques could be successfully applied

86   to seep carbonates (Lalou et al., 1992; Teichert et al., 2003; Kutterolf et al., 2008;

87   Watanabe et al., 2008; Bayon et al., 2009a,b; Liebetrau et al., 2010; Feng et al., 2010;

88   Wirsig et al., 2012; Bayon et al., 2013; Crémière et al., 2013; Tong et al., 2013; Liebetrau

89   et al., 2014; Han et al., 2014; Berndt et al., 2014). Most of these studies have focused on

90   seafloor carbonate crusts, chimneys or chemoherms (Lalou et al., 1992; Teichert et al.,

91   2003; Bayon et al., 2009a,b; Liebetrau et al., 2010; Feng et al., 2010; Wirsig et al., 2012;

92   Bayon et al., 2013; Crémière et al., 2013; Tong et al., 2013; Han et al., 2014), and drilled

93   carbonate mounds (Kutterolf et al., 2008; Liebetrau et al., 2014). To date, only a few

94   investigations have been dedicated to the analysis of buried carbonate nodules at methane

95   seeps (Watanabe et al., 2008; Crémière et al., 2013). Although such approach may offer

96   the opportunity to investigate gas-hydrate dynamics in marine sediments during the Late

97   Quaternary, it can be complicated by diagenetic issues such as dissolution (Luff et al.,

98   2005) and the presence of significant initial ^{230}Th derived from terrigenous material

99   (Watanabe et al., 2008; Bayon et al., 2009; Wirsig et al., 2012), which hence require the

100 use of isochron dating methods.

101

102   In this study, we report U-Th analyses for cm-size nodules of carbonate breccias

103 recovered at various depths from a hydrate-bearing sediment core at the Niger Delta

104 margin. We show below that, when combined with a well-constrained core stratigraphy,

105 this approach can provide unique information on the evolution of gas-hydrate reservoirs

106 and pockmark dynamics through time.

107

108

109 **2. Material and methods**

110

111 *2.1. Regional setting and sampling sites*

112   The Niger Delta is a large sedimentary edifice on the West African margin, which

113 extends southward into the Gulf of Guinea deep basin. In its deep province, gravity

114 tectonism has deformed sediments significantly, leading to folding, diapirism and

115 faulting, all of which have resulted in the migration of gas-rich fluids within continental

116 slope sediments. Numerous occurrences of fluid escape sedimentary structures and gas

117 hydrate deposits have been reported previously on the Niger Delta deep province (Brooks

118 et al., 1994; Bayon et al., 2007; Sultan et al., 2007; Sultan et al., 2010; Bayon et al., 2011;

119 Ruffine et al., 2013; Sultan et al., 2014).

120

121   The pore water, carbonate and sediment samples used for this study were collected by

122 sediment coring during two expeditions on the continental slope off Nigeria in 2003 and

123 2004 (NERIS 1 & 2; chief scientist: M. Voisset). All samples were recovered from a

124 pockmark-rich area of ~ 20 km^2, at about 1200 m water depth (Fig. 1). The geological

setting, occurrence of gas hydrates and geochemical processes related to carbonate precipitation in the study area have been described previously (Bayon et al., 2007; Sultan et al., 2007; Sultan et al., 2010; Rongemaille et al., 2011). This area corresponds to the collapsed summit of an anticline, which is delimited by two deep-rooted normal faults oriented N130. Between those two major faults, the central domain is characterised by the presence of numerous pockmarks of variable shape and diameter (from ~ 10 m to 400 m; see Fig. 1). As discussed in Bayon et al. (2007), apart from the recovery of a few seafloor chemoherm deposits along the major faults, the carbonate samples collected in this central domain correspond almost exclusively to carbonate breccias similar to other gas hydrate-associated carbonates described elsewhere (e.g. Greinert et al., 2001). Geophysical data, sediment coring and geotechnical measurements acquired during the NERIS project revealed that both free gas and gas hydrates occur abundantly in this central domain, in the near-seafloor environment (Sultan et al., 2007). The studied area is located well within the stability field of gas hydrates in the marine environment (Fig. S1). Piston core N2-KS-44 (length 6.6 m; 1174 m water depth) was retrieved from one 15-m deep hydrate-bearing pockmark in this area (Fig. 1). Core lithology is presented in Fig. 2. No evidence for the presence of turbidites or any other mass-transport deposits was encountered in core N2-KS-44. Abundant carbonate concretions were observed between 30 and 180 cm sediment depth, while gas-hydrate nodules occurred deeper in the sediment, below ~ 400 cm (Fig. 2). Hydrate-bearing sediments from a few other cores in the central domain (N1-KSF-23 and N1-KSF-20) and a nearby reference core not affected by any fluid seepage (N1-KSF-39; lat. 3°12.208'N; long. 6°41.003'E; length 10.60 m; 1243 m water depth) were also analysed during this study (Fig. 1).

2.2. Core stratigraphy

In this study, conventional oxygen isotope stratigraphy and AMS radiocarbon dating were not applicable to core N2-KS-44, due to the presence of methane-derived carbonate phases dispersed along the entire core (Bayon et al., 2007). Sedimentary sequences accumulated on the Niger Delta deep province display however large fluctuations in major element composition, which can be used for the purpose of stratigraphic correlation. In particular, the aluminium/titanium (Al/Ti) ratio represents a proxy for past

chemical weathering, related to the alternance of wet and dry periods in the Niger River basin during the Late Quaternary (Zabel et al., 2001). Both Al and Ti are mainly hosted by silicate detrital phases; hence Al/Ti ratios are unlikely to be affected by methane seepage at cold seeps. The age model for core N2-KS-44 was therefore established by tuning its downcore Al/Ti profile to the nearby reference core N1-KSF-39 (Fig. 3). Bulk major element composition of N2-KS-44 and N1-KSF-39 sediments was determined by wavelength-dispersive X-ray fluorescence (WD-XRF) analysis of fusion beads. The chronology for core N1-KSF-39 relies on nine ^{14}C-AMS radiocarbon analyses of mixed planktonic foraminifera fractions (Table 1), and tuning of its Al/Ti profile to the Al/Ti curve of core GeoB4901-8 (Fig. 3); a well-dated sediment record also recovered in the Niger Delta deep province (Zabel et al., 2001). These radiocarbon dates were converted into calendar ages using the Calib 7.1 program (Stuiver et al., 2013), and applying a marine reservoir age of 400 yr. While this approach suffers from inherent uncertainty associated with tuning methods, and especially here with the fact that the Al/Ti profile for core N2-KS-44 is not particularly smooth, the relatively good correlation observed between Al/Ti signals of all three sedimentary records suggest that it can provide, to a first approximation, a reliably good estimate for core N2-KS-44 stratigraphy (Fig. 3). Based on these chronologies, down-core variations in sedimentation rates were calculated for both core N1-KSF-39 (Table 1) and N2-KS-44 (Fig. 3).

2.3. Pore-water analyses

On board, pore waters were extracted from core N2-KS-44 sediments by centrifugation, immediately after sampling, filtered using acetate cellulose filters (0.45 μm diameter) and stored in a refrigerator. Dissolved sulphate (SO_4^{2-}) and chloride (Cl^-) concentrations were measured onshore in 1:10 diluted solutions by ion chromatography. Calcium contents were also determined with an Element2 HR-ICP-MS after simple dilution (between 500 and 1000-fold) with 2% twice sub-boiled nitric acid. Ca concentrations were calculated by external calibration using diluted IAPSO and NASS-5 solutions.

2.4. Petrography and electron microprobe analysis of carbonate breccias

187   Details on the petrography and mineralogy of authigenic carbonate samples recovered
188   at site N2-KS-44 are given in Bayon et al. (2007). Polished sections of selected samples
189   were also examined by scanning electron microscopy (JEOL JSM-840A) and electron
190   microprobe analyzer (JEOL JXA8800R) to provide elemental mapping of carbonate
191   concretions and select sampling areas suitable for U-Th measurements. Authigenic
192   carbonates recovered in the upper two meters of core N2-KS-44 sediments correspond
193   typically to mm- to cm-size carbonate-cemented breccias (Bayon et al., 2007), similar to
194   those reported previously in other hydrate-bearing sediments (Naehr et al., 2000; Greinert
195   et al., 2001). Those carbonate concretions contain intraclasts (biogenic components,
196   mudstones) cemented by aragonite and/or high-Mg calcite (Fig. 4). Some concretions
197   exhibit large (up to ~100 μm diameter) crystals of fibrous aragonite, which have
198   developed in open pore spaces, either between intraclasts or inside the cavities of
199   biogenic components (Fig. 4). Botryoidal aragonite often composes carbonate cements.
200   Numerous intraclasts consist of mudstones cemented by microcrystalline high-Mg
201   calcite, which exhibit a darker color than the surrounding matrix and contain framboidal
202   pyrite. One concretion was recovered in a deeper core section (at 260 cm depth), which
203   corresponds to a homogeneous mudstone cemented by microcrystalline high-Mg calcite
204   (Fig. 2).

205

206   *2.5. Chemical and analytical procedures for U-Th measurements*
207   Selected areas of carbonate concretions from core N2-KS-44 were hand-drilled
208   carefully to obtain samples having weight ranging between 50-100 mg of carbonate
209   powder. However, carbonate breccias are highly heterogeneous and samples of this size
210   (referred to as 'bulk' samples in the following text) are still significantly contaminated by
211   detrital material, with consequences on U-Th dating. Therefore, to try to reduce such
212   contamination, some carbonate samples were also collected using a computer-assisted
213   microsampling device (MicroMill, New Wave Research). This system enables accurate
214   sampling of micrometer-size areas of polished sections. For those small carbonate
215   samples (referred to as 'micromilled' samples subsequently), sampling areas were
216   selected using scanning electron microscopy and/or electron microprobe analyser (Fig.
217   4). Sampling areas were chosen within both aragonite- and high-Mg calcite-rich areas of

218   carbonate breccias. About ~ 1 mg of carbonate powders was collected for each of those
219   micromilled samples for U-Th analysis. A total of six bulk sediment samples containing
220   no visible carbonates were also analysed to characterize the detrital component
221   incorporated within the carbonate concretions.

222

223   The chemical and analytical procedures used in this study largely followed those
224   described in Bayon et al. (2009a). Briefly, each sample (i.e. bulk, micromilled, sediment)
225   was dissolved in 7.5M HNO_3, spiked with a mixed $^{236}U/^{229}Th$ spike, digested in
226   concentrated HNO_3 on the hotplate, and centrifuged. At this stage, any undissolved
227   detrital fractions were transferred into cleaned Teflon vessels and fully digested with a
228   mixed (3:1) HF:HCl solution, before being added back into corresponding supernatants.
229   Samples were evaporated, taken up with 7.5M HNO_3, and diluted with ultrapure water.
230   After Fe-oxide co-precipitation, U and Th were finally separated chemically using
231   conventional anion exchange techniques. The volumes of anion-exchange resin and acids
232   used for separating U-Th were much smaller for micromilled samples than for bulk and
233   sediment samples. Typical procedural blanks were 1.2×10^{-10} g ^{238}U and 3.0×10^{-11} g
234   ^{232}Th for bulk carbonate and sediment samples, and 1.0×10^{-11} g ^{238}U and 1.3×10^{-12} g
235   ^{232}Th for micromilled samples. Total U and Th procedural blanks were small compared
236   to final sample concentrations. U and Th concentrations and isotope ratios were
237   measured with a MC-ICPMS (Nu Plasma). The external reproducibility on the $^{234}U/^{235}U$
238   ratio was assessed by measuring repeatedly the standard CRM-145 during each session
239   using a standard-bracketing measurement protocol. Th was measured with ^{229}Th and
240   ^{230}Th sequentially in a single ion-counter equipped with an energy filter to improve
241   abundance sensitivity, and ^{232}Th in a Faraday collector. Precision obtained on measured
242    $^{229}Th/^{230}Th$ ratios was always better than 5 ‰ for bulk and sediment samples, and 50 ‰
243   for micromilled samples. Blank correction on ^{230}Th concentrations was calculated using
244   measured $^{232}Th/^{230}Th$ ratio and ^{232}Th concentration for blank. For the small-size
245   micromilled samples, blank contributions accounted for between 0.7% (N2-KS-44_75-1)
246   to 9.3% (N2-KS-44_180-1).

247

248

249 **3. Results**

250

251 *3.1. Pore-water SO_4^{2-}, Cl^- and Ca^{2+} profiles*

252   For core N2-KS-44, pore water SO_4^{2-} concentrations display seawater-like values from

253 the surface sediment to 60 cm depth, and then decrease steadily to reach near-zero values

254 from 260 cm depth to downcore (Fig. 2). Dissolved calcium concentrations show a

255 relatively similar downcore profile, characterized by a significant drop from $\sim$ 10 mM

256 (i.e. seawater values) in the upper sediment layers to about 1 mM. In contrast, chloride

257 concentrations exhibit little variation along the upper section of core N2-KS-44 ($\sim$ 560 $\pm$

258 22 mM).

259

260 *3.2. Electron microprobe elemental distribution maps*

261   The chemical maps obtained by electron microprobe analyser for one representative

262 carbonate breccia from core N2-KS-44 (collected at 160 cm depth) are presented in Fig.

263 5. The Si distribution map can be used to infer the extent to which carbonate cements

264 may be contaminated by detrital material (e.g. clays). Aragonite exhibits typically higher

265 levels of Sr than high-Mg carbonates (Fig. 5). In Fig. 5, it is also clear that aragonite-rich

266 areas are much less contaminated by detrital material (i.e. lower Si contents) than high-

267 Mg calcite-rich mudclasts and cements. We showed earlier that contamination by

268 terrigenous material in cold-seep carbonates increased as the size of crystals in the

269 carbonate cement decreases (Bayon et al., 2007). In those carbonate-cemented breccias

270 from core N2-KS-44, large fibrous crystals of aragonite, developed in open pore spaces

271 and cavities, contain much less detrital material (< 2 wt % Si contents) than botryoidal

272 aragonite (< 2.5 % Si), microcrystalline aragonite (< 5 % Si), and microcrystalline high-

273 Mg calcite (up to 7 % Si). In Fig. 5, this is demonstrated by the evidence that fibrous

274 aragonite-rich areas, such as those encountered in open cavities, contain very low levels

275 of Si. Importantly, concerning U-Th dating, this also indicates that it is best to sample

276 well-crystallised aragonite-rich areas in order to reduce contamination by detrital

277 material.

278

279 *3.3. Uranium and thorium concentrations and isotopic ratios*

280   U-Th data for sediments and authigenic carbonates are listed in Table 2.   U

281   concentrations vary between ~ 5-17 ppm and ~ 2-23 ppm for sediments and carbonates,

282   respectively. ^{230}Th concentrations range from 5 to 62 ppt (mean average of 33 ppt) in

283   authigenic carbonates and from 80 to 105 ppt in sediments.   Carbonate (^{230}Th/^{232}Th)

284   ratios (brackets indicate activity ratios) are low (from 1.2 to 5.3; Table 3), due to both the

285   young formation age of carbonates (low ^{230}Th ingrowth) and detrital contamination (high

286   initial ^{232}Th).   Micromilled samples for aragonite-rich concretions exhibit higher

287   (^{238}U/^{232}Th) ratios (from 6.4 to 32.3; Table 2) than sediments (from 1.2 to 4.4; Table 2)

288   and corresponding bulk carbonates (from 5.2 to 20.6; Table 2).   This indicates that

289   micromilling has been successful in sampling carbonate with lower detrital contents.   In

290   contrast, Mg-rich carbonates generally display comparatively lower (^{230}Th/^{232}Th) and

291   (^{238}U/^{232}Th) ratios even in micromilled subsamples, reflecting both the fact that calcite is

292   less enriched in U compared to aragonite, and that high-Mg microcrystalline carbonate

293   phases are more enriched in detrital components (Bayon et al., 2007).

294

295   *3.4. U-Th isochron dating*

296   Isochron dating methods consider each sample to be composed of a mixture of two

297   components.   In this case, they can be used to separate ^{230}Th present initially from that

298   ingrown from U in the carbonate.   By analysing several subsamples of the same age but

299   with different proportions of the two components, it is possible to calculate the age

300   corresponding to the end-member with no initial ^{230}Th (Edwards et al., 2003).   In seep-

301   related studies, this approach may be complicated by the fact that authigenic concretions

302   may have recorded several discrete events of carbonate precipitation.   In this case,

303   isochron methods may also prove to be particularly useful for assessing whether studied

304   concretions are polygenic or instead correspond to single precipitation events.   In this

305   study, we have considered a sediment end-member, assumed to be representative of the

306   initial sediment fraction incorporated by carbonate breccias.   The U-Th isotopic

307   composition of this sediment fraction can be influenced by its mineralogical composition

308   and the amount of incorporated hydrogenous ^{230}Th derived from the overlying water

309   column.   Using a typical sediment end-member to correct ages is more appropriate than

310   correcting each sample with a sediment measurement from the same core.   The latter

311 approach would generate isochrons containing two high-precision data points, leading to
312 unrealistically precise calculated ages which do not incorporate any uncertainty due to
313 possible variability in the sediment. The approach of defining a typical sediment end-
314 member for one given area circumvents this problem and leads to larger but more
315 realistic age uncertainties, thereby allowing calculation of less precise but more accurate
316 ages. Another possible approach would have been to consider a sediment end-member
317 assumed to be at secular equilibrium, i.e. with activity ratios of 1.0 ± 0.5 (e.g. Bayon et
318 al., 2013). While it may seem more appropriate to apply a regional sediment end-
319 member for correction, note that the use of a theoretical end-member would have led to
320 the same conclusions, yielding very similar isochron ages (always within ~25%). In this
321 study, the sediment end-member has been defined as the average ($\pm$ 1 SD) of six
322 sediments from our study area (Table 3). All these sediments were recovered from
323 seepage sites and hence can be considered, to a first approximation, as representative of
324 the sediment incorporated by the studied carbonate concretions, even in the eventuality
325 that circulation of methane-rich fluids may alter the U-Th isotopic composition of the
326 sediment. On a (^{230}Th/^{232}Th) versus (^{238}U/^{232}Th) plot (Fig. S2), these sediments are
327 clustered near the equiline, with typical crustal values (~ 1.0). This indicates a
328 reasonably homogeneous source of initial Th for carbonate breccias in the studied area,
329 and suggests that isochron dating using this sediment end-member is suitable.
330
331 Isochron diagrams and ages obtained with the sediment end-member are presented in Fig.
332 6 and Table 3. Isochron ages were calculated with Isoplot-Ex 3.70 (Ludwig, 2008), using
333 measured (^{232}Th/^{238}U), (^{230}Th/^{238}U) and (^{234}U/^{238}U) ratios (Table 3). The ^{230}Th/U age
334 errors were calculated by a Monte Carlo simulation, rather than from the first-derivative
335 expansion which led, in the case of this study, to unrealistically small errors. However,
336 when the use of Monte Carlo solution was not possible, an arbitrary error of $\pm$ 25% was
337 assigned to the obtained isochron ages. This arbitrary error corresponds to the external
338 reproducibility on isochron ages estimated from repeated analyses of an in-house cold
339 seep carbonate standard (Bayon et al., 2013).
340

341   In Table 3, two isochron ages are reported: 1) two-point (n=2) isochron ages, which

342   provide an age estimate for every analysed sample; and 2) pseudo-isochron ages (with

343   n>2) that integrate, for any given concretion, all the studied sub-samples. As can be seen

344   in Fig. 6 (Osmond isochron diagrams), except for the concretion at 75cm depth, the

345   distinct fractions (e.g. bulk concretion, micromilled carbonate phases, associated

346   sediment, average composition of the local sediment) associated with carbonate breccias

347   are remarkably well aligned along pseudo-isochron slopes, suggesting that they formed

348   cogenetically. Importantly, this observation also provides strong support for the validity

349   of calculated pseudo-isochron ages and indicates adequate correction of contamination

350   from inherited Th. In contrast, the studied subsamples from the concretion at 75 cm

351   depth are not aligned in Fig. 6, suggesting that they probably did not form

352   contemporaneously (see discussion below). In this case, only the two-point isochron ages

353   will hence be considered in the following discussion.

354

355   Within error (2s), most carbonate breccias display isochron corrected $\delta^{234}U_{(T)}$ values

356   similar to seawater values ($\delta^{234}U$ = 146.6 ± 2.5 ‰ (Robinson et al., 2004; Table 3),

357   suggesting that they formed in the near-seafloor environment. The calculated isochron

358   ages range from 4.8 ± 1.4 to 15.6 ± 1.6 thousand years before present (ka; or ka). All

359   analysed samples (bulk, micromilled, associated sediment) for the upper carbonate-rich

360   layer at 30 cm depth yield a pseudo-isochron age of 8.5 ± 0.2 ka (n = 4; i.e. four-point

361   isochron). Isochron ages of 9.4 ± 2.4 (n = 5) and 10.8 ± 2.7 ka (n = 3) were also obtained

362   for carbonate breccias collected at 160cm and 180cm, respectively. The three carbonate

363   samples (bulk, micromilled-1, micromilled-2) analysed for the sediment layer at 75 cm

364   depth define two-point isochron ages of 9.3 ± 2.0 ka, 12.4 ± 1.3 ka and 4.8 ± 1.4 ka,

365   respectively. Finally, the two bulk samples from the homogeneous nodule of high-Mg

366   calcite at 260 cm gives a pseudo isochron age of 15.6 ± 1.6 ka (n = 3).

367

368

369   **4. Discussion**

370

371   *4.1. Present-day SMTZ and associated carbonate precipitation*

372   In cold seep environments, AOM occurs typically within a localized horizon in marine

373   sediments, called the sulphate-methane transition zone (SMTZ), where both SO_4^{2-} and

374   CH_4 are consumed by microbial assemblages (Reeburg, 1976; Boetius et al., 2000).

375   Other biogeochemical processes, such as the degradation of organic matter (Froelich et

376   al., 1979), or the consumption of C_{2+} hydrocarbon compounds (Joye et al., 2004), may

377   also consume SO_4^{2-} from pore waters in marine sediments. However, at cold seeps,

378   AOM is generally the main process controlling sulphate depletion, leading to near-

379   complete SO_4^{2-} depletion at the SMTZ depth (Niewöhner et al., 1998; Borowski et al.,

380   1999) and producing pseudo-linear SO_4^{2-} profiles in pore-waters, similar to what can be

381   observed at site N2-KS-44 (Fig. 2). In hydrate-bearing settings, the SMTZ depth is also

382   often correlated with the occurrence of gas hydrate within the sediment (e.g. Borowski et

383   al., 1999). In the study area, this feature is nicely illustrated when plotting the SMTZ

384   depth versus the depth of occurrence of gas hydrate layers within distinct sediment cores,

385   which both define a very good correlation (Fig. 7). Gas hydrates generally hamper the

386   ascent of fluids and reduce their transport towards the seafloor (e.g. Sultan et al., 2010; Li

387   et al., 2014; Crutchley et al., 2015). However, without gas supply to sustain their

388   formation, hydrates dissolve away to stay in thermodynamic equilibrium with

389   surrounding pore waters (e.g. Ecker et al., 1998). This dissolution process contributes to

390   permanent supply of methane to pore waters above gas hydrate layers, acting as a driving

391   force for the AOM reaction coupled with sulphate reduction (Sultan et al., 2010, 2014).

392   Note that the 'dissolution' process that we refer to here differs from 'dissociation', which

393   generally occurs whenever gas hydrates leave their temperature-pressure stability field, in

394   response for example to a sea-level drop or a rise in bottom-water temperature.

395

396   At site N2-KS-44, the profile for pore-water Ca^{2+} concentrations also shows a strong

397   depletion at ~3.6 m depth (Fig. 2), which indicates that active carbonate precipitation is

398   currently taking place at the depth of present-day SMTZ. This is in full agreement with

399   evidence for the presence of dispersed high-Mg calcite phases at this depth in core N2-

400   KS-44, inferred from modelling of bulk sediment Sr/Ca and Mg/Ca ratios (Bayon et al.,

401   2007). Overall, our pore water data indicate that the present-day AOM and associated

402   authigenic carbonate precipitation occurs at depth close to 3 m in core N2-KS-44, hence

403　much deeper than the overlying carbonate-rich layer of authigenic concretions

404　encountered between ~ 30 and 180 cm depth.

405

406　*4.2. A major event of carbonate precipitation between ~13.0 and 2.5 ka*

407　　The comparison of U-Th isochron ages for carbonate-cemented breccias with their

408　corresponding stratigraphic age (inferred from Al/Ti tuning) can provide temporal

409　constraints on the formation of the carbonate-rich layer located in the upper two meters of

410　core N2-KS-44. Stratigraphically, this horizon corresponds to the approximate time

411　interval 2.5-13.0 ka, which hence overlaps relatively well the observed range of

412　calculated U-Th ages for carbonate breccias from 4.8 ± 1.4 to 12.4 ± 1.3 ka (Fig. 8). This

413　observation suggests that the carbonate-breccias were formed in close proximity to the

414　seafloor. This hypothesis is supported by the evidence that the carbonate breccias

415　collected at 75 cm (for the micromilled-2 subsample), 160 cm and 180 cm depth provide

416　U-Th isochron ages similar (within error) to their corresponding stratigraphic age (Fig.

417　8). Another argument in favor of a near-seafloor precipitation is the presence of

418　aragonite, which is generally favored over that of calcite at high SO_4^{2-} concentrations or

419　when uprising fluids have a high velocity flow, hence whenever AOM proceeds in the

420　near-seafloor environment (e.g. Burton, 1993; Aloisi et al., 2000; Luff and Wallman,

421　2003; Bayon et al., 2009a).

422

423　　In contrast, the two carbonate breccias from the upper carbonate-rich layer, i.e. those

424　collected at 30 cm and 75 cm depth (with the exception of the micromilled-2 subsample),

425　display isochron ages older than their respective stratigraphic age (Fig. 8), indicating

426　possible sediment reworking. An interesting feature of our results is also the evidence for

427　the presence of polygenic breccias. The two micromilled samples from the concretion

428　collected at 75 cm depth display distinct U-Th isochron ages (12.4 ± 1.3 ka and 4.8 ± 1.4

429　ka), which suggests that such breccias may have recorded several precipitation events. In

430　this context, the bulk sample (9.3 ± 2.0 ka) analysed for that particular carbonate breccia

431　most likely corresponds to a mixture between distinct polygenic carbonate phases. For

432　this particular concretion, the fact that the high-Mg rich micromilled sample appears to be

433　younger than the aragonite one could possibly indicate that high-Mg carbonate phases

434   preferentially formed after an initial event of aragonite precipitation, perhaps after

435   subsequent burial of concretions within the sediment. At this stage, petrographic

436   examination does not reveal any clear succession of different carbonate precipitation

437   events that could possibly explain the observed age/mineralogical differences in the

438   studied breccias (Fig. 4). In fact, some high-Mg rich micro-concretions observed in the

439   studied carbonate breccias (see Fig. 4e) even appear to be older than corresponding

440   aragonite cement, which would go in opposite direction to what can be proposed based

441   on our U-Th dates for the two micromilled samples at 75 cm depth. The observed

442   complex nature of the studied carbonate breccias clearly show that a much larger U-Th

443   investigation of additional micromilled samples from the same core would be needed to

444   identify whether distinct carbonate precipitation events occurred during the last few

445   thousand years. In addition, one cannot exclude that other breccias present in this core

446   section are older or younger than those analysed in this study. Therefore, to a first

447   approximation, and despite indications for a potentially more complex formation

448   scenario, the comparison of U-Th isochron ages for carbonate-cemented breccias with

449   their corresponding stratigraphic age suggest that carbonate formation at site N2-KS-44

450   was probably active in the near-seafloor environment during a relatively well-defined

451   time interval, between about 13 and 2.5 ka.

452

453   *4.3. Constraints on pockmark dynamics*

454   As mentioned above, the evidence that a few carbonate breccias exhibit U-Th ages

455   significantly older than their corresponding stratigraphic age suggests that sediment

456   reworking may have taken place at site N2-KS-44. Further constraints on pockmark

457   evolution at the studied site can also be obtained by comparing carbonate U-Th ages with

458   the sediment accumulation rates inferred for cores N2-KS-44 and N1-KSF-39 (Fig. 8).

459   From ~ 30 to 13 ka, the two neighbour cores were characterized by similar sedimentation

460   rates, in the range ~ 4-10 cm/kyr, thereby suggesting a similar depositional context.

461   However, after 13 ka, sedimentation rates at the two sites started to be decoupled.

462   Between about 13 and 7 ka, the reference site (N1-KSF-39) experienced rapidly

463   increasing sedimentation rates (up to ~ 23 cm/kyr), probably in relation with much higher

464   fluvial discharges from the Niger River basin (Pastouret et al., 1978; Zabel et al., 2001),

465 before returning to much lower sediment accumulation after 7 ka (about 5 cm/kyr). In

466 contrast, at site N2-KS-44, sedimentation rates remained relatively low (below 8 cm/kyr)

467 until about 10 ka, before increasing steadily to about 18 cm/kyr for the remaining

468 Holocene period. To account for the observed decoupling, we propose that intense

469 circulation of methane-rich fluids near the seafloor led to highly dynamic seafloor

470 environment at site N2-KS-44 between ~ 13 to 10 ka (Fig. 9b). This event would have

471 resulted in seafloor carbonate precipitation, but also in intense fluid seepage and

472 associated particle resuspension or sediment winnowing (Fig. 9b). Instead, from 10 ka

473 onwards, the shift towards enhanced sedimentation rates at site N2-KS-44 could possibly

474 be related to a second evolutionary stage of the pockmark, characterized by collapse

475 depression (Fig. 9c). Recent studies have shown that pockmarks and other seafloor

476 depressions are often characterized by higher sedimentation rates compared to the

477 surrounding seafloor (e.g. Pau and Hammer, 2013; Pau et al., 2014). The same studies

478 have also shown that sedimentation patterns at pockmarks are typically associated with

479 deposition of coarse-grained material, transported as bedload. Based on the above

480 consideration, one hypothesis would be that the presence of carbonate concretions older

481 than corresponding stratigraphic ages in the upper carbonate-rich layer relates to

482 subsequent reworking of small carbonate breccias during the period that followed intense

483 fluid seepage. This would mean that some of the studied concretions in the upper

484 aragonite-rich layer of core N2-KS-44 may be derived from the erosion of the

485 surrounding seafloor, perhaps in response to the deepening of the pockmark (Fig. 9c).

486 Another argument that would support sediment reworking after 10 ka would be the

487 'sawtooth' Al/Ti profile along core N2-KS-44, which contrasts with the much smoother

488 Al/Ti curves observed at reference sites N1-KSF-39 and GeoB4901-8 (Fig. 3).

489

490 *4.4. Evidence for fluctuating SMTZ over the last 15 ka*

491   In contrast with the breccias from the upper carbonate-rich layer, the homogeneous

492 nodule of high-Mg calcite collected at 260 cm depth appears to be significantly younger

493 (15.6 ± 1.6 ka) than its corresponding estimated stratigraphic age (about 24 ka; Fig. 8).

494 Considering the average sedimentation rate inferred from our Al-Ti-tuned age model for

495 that section of core N2-KS-44 (~ 7.3 cm/kyr; Fig. 3), we can estimate that this nodule

496 formed at about 60 cm below the seafloor. This would explain why it is mainly composed

497 of high-Mg calcite rather than aragonite, which more commonly precipitates at the

498 sediment-seawater interface.

499

500   As mentioned above (section 4.1), the depth at which AOM and associated carbonate

501 precipitation occurs in hydrate-bearing sediments of the study area is controlled primarily

502 by the occurrence depth of gas hydrate layers (Fig. 7). Most likely, during the Holocene,

503 both AOM and associated carbonate precipitation took place near the seafloor at site N2-

504 KS-44, thereby explaining the formation of the aragonite-rich layer that is currently

505 located between 30 cm and 180 cm depth. Instead, our U-Th data for the carbonate

506 nodule at 260 cm depth suggest that the paleo-SMTZ at about 15.6 ka was probably

507 located deeper in the sediment column (about 60 cm depth; Fig. 9a). Taken together with

508 our pore-water analyses and inferred depth for the present-day SMTZ (i.e. about 300 cm

509 depth), these data hence indicate methane fluxes must have fluctuated significantly over

510 the last 15 kyr at the studied site (Fig. 9).

511

512 *4.5. Factors controlling gas hydrate dynamics and associated CH$_4$ fluxes in Niger Delta*

513 *sediments*

514   Field observations and measurements have shown that the distribution of gas hydrates

515 within sediments is highly heterogeneous in hydrate-bearing areas, both at small (meter)

516 and regional scales (Tréhu et al., 2004; Sultan et al., 2007). Gas hydrates are found

517 typically in meter-thick patchy zones in marine sediments (Kvenvolden and Lorenson,

518 2001; Tréhu et al., 2004). In Niger Delta sediments, such a large heterogeneity for gas

519 hydrate distribution was confirmed by geophysical surveying and coring during the

520 NERIS expeditions (Sultan et al., 2007) and subsequent cruises (Sultan et al., 2010;

521 Sultan et al., 2014; Wei et al., 2015). It is likely, therefore, that variations in upward

522 methane fluxes from one site to another are controlled primarily by the heterogeneous

523 distribution of gas hydrates within sediments, or the presence of faults acting as a major

524 methane conduit. Considering a given hydrate-bearing site (e.g. Site N2-KS-44),

525 however, it is expected that changes in the CH$_4$ flux over time are caused by parameters

526 affecting the dynamic of gas-hydrate deposits, such as changes in e.g. hydrostatic

527   pressure, bottom-water temperature, slope stability, and *in situ* CH_4 flux and/or

528   concentration at the base of the gas-hydrate occurrence zone (GHOZ) within the

529   sediment. Below, we investigate whether each of those four different factors may have

530   accounted for the inferred fluctuations of the SMTZ depth (and associated methane

531   fluxes) at site N2-KS-44.

532

533   Sea-level rise since the last 15,000 years is unlikely to have led to gas-hydrate

534   dissociation in Niger Delta sediments. Instead, increasing hydrostatic pressure at that

535   time contributed most probably to an opposite effect, i.e. greater gas hydrate stability in

536   sediments. Alternatively, reorganization of intermediate-water circulation during the

537   Holocene period could have induced an increase in bottom-water temperatures, leading to

538   partial dissociation of hydrate layers in sediments (see Fig. S1). This would need to be

539   tested in future studies, but at present, to the best of our knowledge, there is no evidence

540   for deep-sea temperature changes over glacial-interglacial timescales in the Tropical

541   Atlantic for the water depth considered in this study. Sedimentation rates were

542   apparently higher on the Niger deep-sea fan between 13 to 10 ka, as shown by our own

543   data (Table 1) and in agreement with previous studies (Pastouret et al., 1978; Zabel et al.,

544   2001). This was due probably to high fluvial discharges at the onset of the so-called

545   Holocene thermal maximum (~ 11-6 ka) in subtropical Africa, i.e. a progressive climatic

546   shift towards warmer and wetter conditions related to maximum summer insolation. This

547   could have possibly triggered slope failures and, in turn, to destabilization of gas hydrate

548   reservoirs within sediments. However, in absence of any evidence for sediment

549   instabilities in the studied area, higher sedimentation rates at that time led most likely to

550   even greater hydrate stability instead.

551

552   Based on the above, we argue that the inferred variation of methane fluxes at site N2-

553   KS-44 has not been driven by external parameters during the last 15,000 years, but

554   instead by internal processes. Previous studies have already suggested that local fluid

555   flow dynamics was likely to explain both the evolution of gas-hydrate reservoirs and

556   associated pockmarks (Cathles et al., 2010; Sultan et al., 2010; Sultan et al., 2014). In

557   this area, the occurrence of gas hydrate reservoirs in sub-surface sediments is related to

558 high fluid pressure in the deeper sedimentary column, and associated migration of both

559 free gas and methane-rich fluids along fractures (Sultan et al., 2014). Periodically, as a

560 consequence of enhanced fluid flow, gas hydrate fronts can move both upwards and

561 laterally in shallower sediments. Therefore, at site N2-KS-44, the period of intense fluid

562 activity after 13 ka inferred from our data hence probably corresponds to a particular

563 episode of high free gas and fluid pressure at the base of the GHOZ, which led to gas-

564 hydrate formation near the seafloor.

565

566 *4.6. Implications on the evolution of hydrate-bearing pockmarks through time*

567 The timing of pockmark formation has been often discussed in previous studies, in

568 particular through the application of U-Th dating to cold seep carbonates. Carbonate U-

569 Th investigations conducted at various seeps worldwide (e.g. Gulf of Mexico, Japan Sea,

570 Black Sea, Congo margin, Hikurangi margin, South China Sea) have led to the

571 suggestion that pockmark formation often took place during low sea-level stands in the

572 past (Watanabe et al., 2008; Feng et al., 2010; Liebetrau et al., 2010; Tong et al., 2013;

573 Han et al., 2014). The reduced hydrostatic pressure that has accompanied previous sea-

574 level falls is thought to have resulted in both enhanced fluid flow and hydrate

575 dissociation, which ultimately led to pockmark formation and authigenic carbonate

576 precipitation. Other factors have been also evoked as possible mechanisms accounting

577 for past hydrate destabilisation events and/or pockmark formation, which include e.g.

578 changes in bottom water temperatures (Mienert et al., 2005; Ménot and Bard, 2010;

579 Berndt et al., 2014; Pau et al., 2014), dissolved sulfate contents (Crémière et al., 2013),

580 seismic activity (Liebetrau et al., 2010; Fischer et al., 2013). In our study, as discussed

581 above and in agreement with earlier works (Sultan et al., 2010; Sultan et al., 2014), gas

582 hydrate and pockmark dynamics have been probably mainly driven by internal factors, at

583 least over the last few thousand years. At a longer time scale, of course, one cannot

584 exclude that external parameters such as sea-level changes also played an important role

585 in controlling fluid seepage intensity in the Niger delta area, especially at seep sites

586 located at shallower water depths.

587

588   In marked contrast, very little information exists about the evolution of hydrate-bearing

589   pockmarks through time. This is simply because such information can only be derived

590   from numerical modeling (e.g. Sultan et al., 2010) or analytically challenging high-

591   resolution U-Th investigations of authigenic carbonate deposits or buried concretions

592   along sediment cores (Watanabe et al., 2008; Crémière et al., 2013). In this regard, our

593   study provides interesting constraints about the duration and evolution of hydrate-bearing

594   pockmark at margins.

595

596   Our results first suggest that the presence of gas hydrate reservoirs near the seafloor can

597   sustain continuous methane seepage and associated carbonate precipitation for several

598   thousand year long periods of time. Interestingly, at site N2-KS-44, the duration of this

599   event of enhanced seepage activity and gas-hydrate growth, associated carbonate

600   precipitation, and subsequent hydrate dissolution inferred from our results (i.e. about

601   10,000 years) agrees relatively well with estimates obtained by numerical modeling for

602   the same study area (about 8,000 years; Sultan et al., 2010). In this latter work, the

603   calculated duration corresponded to the period of gas hydrate dissolution that followed a

604   sudden theoretical cessation of methane supply from the underlying sediment column.

605   While gas hydrates may form rapidly, their long-term preservation in sub-surface

606   sediments is indeed ultimately controlled by the sustainability of methane inputs from

607   deeper sediments (Sultan et al., 2014). Gas-hydrate dissolution occurs whenever the

608   methane flux and/or concentration at the base of the GHOZ decreases. The upper layers

609   of gas hydrate reservoirs are generally those that start dissolving first in response to a

610   local decrease of methane fluxes (Sultan et al., 2010). Hydrate dissolution generally

611   leads to an increase of pore-water pressure and, in turn, to sediment collapse and

612   pockmark formation (Sultan et al., 2010; Sultan et al., 2014). In this context, the inferred

613   mode of gas hydrate evolution can be referred to as rapid hydrate growth versus slow

614   hydrate dissolution (Sultan et al., 2014). This latter model that links hydrate dynamics

615   and the evolution of pockmark through time agrees very well with our own observations

616   based on carbonate U-Th dating and inferred sedimentation rates (Fig. 9). Based on our

617   data alone, however, it would remain difficult to argue whether the observed pockmark

618   evolution at site N2-KS-44 and the recent deepening the SMTZ inferred from our pore-

619   water data are related to a sudden, or instead a progressive, decrease of methane fluxes.

620

621

622   **5. Concluding remarks**

623

624   In this study, we have been able to reconstruct the temporal evolution of gas hydrate

625   deposits and associated methane fluxes at a pockmark on the Niger Delta margin, using

626   an original approach based on: 1) U-Th dating of methane-derived carbonate breccias

627   collected at various depths along a sediment core, 2) the determination of corresponding

628   stratigraphic ages and inferred sedimentation rates, and 3) acquisition of pore water data.

629   At the studied location, a major episode of carbonate precipitation occurred between

630   about 13.0 and 2.5 ka, probably triggered by the upward migration of gas hydrate

631   reservoirs to near the seafloor. Enhanced methane fluxes in the upper sediment layers

632   were probably first accompanied with intense fluid seepage and sediment winnowing at

633   the seafloor. After this initial phase, we propose that hydrate dissolution prevailed in

634   sub-surface sediments, probably in response to decreasing methane fluxes at the base of

635   the local gas hydrate occurrence zone. Presumably, this would have led to pockmark

636   formation and the deepening of the sulphate-methane transition zone, in agreement with

637   evidence from present-day pore-water data. This would also be supported by evidence for

638   rapidly increasing sedimentation rates at the same time and the presence of carbonate

639   concretions older than corresponding stratigraphic ages, which both suggest sediment

640   erosion and/or reworking.

641

642   Similarly to what has been previously proposed for the same area based on numerical

643   modeling, our results suggest that the activity of pockmarks in the Niger Delta area is

644   strongly related to gas hydrate dynamics. In future work, the methodology developed in

645   this study could provide interesting insights into the co-evolution of gas hydrate

646   reservoirs and pockmarks at margins. In particular, high-resolution U-Th studies of cold

647   seep carbonates from hydrate-bearing areas should aim at further investigating the

648   resilience of gas hydrate reservoirs and associated pockmark activity to past

649 environmental changes, especially in the context of ongoing global warming and its

650 potential impact on submarine gas hydrate reservoirs.

651

652

REFERENCES

Aloisi, G., Pierre, C., Rouchy, J.M., Foucher, J.P., Woodside, J., the MEDINAUT Scientific Party, 2000. Methane-related authigenic carbonates of eastern Mediterranean Sea mud volcanoes and their possible relation to gas hydrate destabilisation. Earth Planet. Sci. Lett. 184, 321–338.

Bangs, N.L., Hornbach, M.J., Moore, G.F., Park, J.-O, 2010. Massive methane release triggered by seafloor erosion offshore southwestern Japan. Geology 38, 1019-1022.

Bayon, G., Pierre, C., Etoubleau, J., Voisset, M., Cauquil, E., Marsset, T., Sultan, N., Le Drezen, E., Fouquet, Y., 2007. Sr/Ca and Mg/Ca ratios in Niger Delta sediments: Implications for authigenic carbonate genesis in cold seep environments. Mar. Geol. 241, 93-109.

Bayon, G., Henderson, G.M., Bohn, M., 2009a. U-Th stratigraphy of a cold seep carbonate crust. Chem. Geol. 260, 47-56.

Bayon, G., Loncke, L., Dupré, S., Caprais, J.-C., Ducassou, E., Duperron, S., Etoubleau, J., Foucher, J.-P., Fouquet, Y., Gontharet, S., Henderson, G.M., Huguen, C., Klaucke, I., Mascle, J., Migeon, S., Olu-Le Roy, K., Ondréas, H., Pierre, C., Sibuet, M., Stadnitskaia, A., Woodside, J., 2009b. Multi-disciplinary investigation of fluid seepage on an unstable margin: The case of the Central Nile deep sea fan. Mar. Geol. 261, 92-104.

Bayon, G., Birot, D., Ruffine, L., Caprais, J.C., Ponzevera, E., Bollinger, C., Donval, J.P., Charlou, J.L., Voisset, M., Grimaud, S., 2011. Evidence for intense REE scavenging at cold seeps from the Niger Delta margin. Earth Planet. Sci. Lett. 312, 443-452.

Bayon, G., Dupré S., Ponzevera, E., Etoubleau, J., Chéron, S., Pierre, C., Mascle, J., Boetius, A., de Lange G., 2013. Formation of carbonate chimneys in the Mediterranean Sea linked to deep-water oxygen depletion. Nat. Geosci. 6, 755-760.

Berndt, C., Feseker, T., Treude, T., Krastel, S., Liebetrau, V., Niemann, H., Bertics, V.J., Dumke, I., Dünnbier, K., Ferré, B., Graves, C., Gross, F., Hissmann, K., Hühnerbach,

V., Krause, S., Lieser, K., Schauer, J., Steinle, L., 2014. Temporal Constraints on Hydrate-Controlled Methane Seepage off Svalbard. Science 343, 284–287.

Bohrmann, G., Meinert, J., Suess, E., Torres, M., 1998. Authigenic carbonates from the Cascadia subduction zone and their relation to gas hydrate stability. Geology 26, 647-650.

Boetius, A., Ravenschlag, K., Schubert, C.J., Rickert, D., Widdel, F., Gieseke, A., Amann, R., Jorgensen, B.B., Witte, U., Pfannkuche, O., 2000. A marine microbial consortium apparently mediating anaerobic oxidation of methane. Nature 407, 623-626.

Borowski, W.S., Paull, C.K., Ussler III, W., 1999. Global and local variations of interstitial sulphate gradients in deep-water, continental margin sediments: Sensitivity to underlying methane and gas hydrates. Mar. Geol. 159, 131-154.

Brooks, J.M., Anderson, A.L., Sassen, R., MacDonald, I.R., Kennicutt II, M.C., Guinasso Jr., N.L., 1994. Hydrate occurrences in shallow subsurface cores from continental slope sediments. In Annals of the New York Academy of Sciences 715, 381-391.

Buffett, B.A., 2000. Clathrate hydrates. Annu. Rev. Earth Planet. Sci. 28, 477-507.

Burton, E.A., 1993. Controls on marine carbonate cement mineralogy: review and reassessment. Chem. Geol. 105, 163–179.

Cathles, L.M., Su, Z., Chen D., 2010. The physics of gas chimney and pockmark formation, with implications for assessment of seafloor hazards and gas sequestration. Mar. Petrol. Geol. 27, 82-91.

Crémière, A., Bayon, G., Ponzevera, E., Pierre, C., 2013. Paleo-environmental controls on methane-derived carbonate authigenesis in the Sea of Marmara. Earth Planet. Sci. Lett. 376, 200-211.

Crutchley, G. J., Fraser, D. R. A., Pecher, I. A., Gorman, A. R., Maslen, G., Henrys, S. A., 2015. Gas migration into gas hydrate-bearing sediments on the southern Hikurangi margin of New Zealand. J. Geophys. Res. Solid Earth 120, 725-743.

Davy, B., Pecher, I.A., Wood, R., Carter, L., Gohl, K., 2010. Gas escape features off New Zealand – Evidence for a massive release of methane from hydrates. Geophys. Res. Let. 37, L21309.

de Prunelé, A., Ruffine, L., Riboulot, V., Peters, C.A., Croguennec, C., Guyader, V., Pape, T., Bollinger, C., Bayon, G., Caprais, J.C., Donval, J.P., Marsset, T., Bohrmann, G., Géli, L., Rabiu, A., Lescanne, M., Cauquil, E., Sultan, N., 2015. Focused hydrocarbon-migration in shallow sediments of a pockmark cluster in the Niger Delta. Mar. Petrol. Geol. (submitted).

Dickens, G.R., O'Neil, J.R., Rea, D.K., Owen, R.M., 1995. Dissociation of oceanic methane hydrate as a cause of the carbon isotope excursion at the end of the Paleocene. Paleoceanog. 10, 965-971.

Dickens, G.R., 2003. Rethinking the global carbon cycle with a large, dynamic and microbially mediated gas hydrate capacitor. Earth Planet. Sci. Lett. 213, 169-183.

Ecker, C., Dvorkin, J., Nur, A., 1998. Sediments with gas hydrates: Internal structure from seismic AVO. Geophysics 63, 1659-1669.

Edwards, R.L., Gallup, C.D., Cheng, H., 2003. Uranium-series dating of marine and lacustrine carbonates. Rev. Min. Geochem. 52, 363-405.

Feng, D., Roberts, H.H., Cheng, H., Peckmann, J., Bohrmann, G., Edwards, R.L., Chen, D., 2010. U/Th dating of cold-seep carbonates: an initial comparison. Deep Sea Res. II, 57, 2055-2060.

Fischer, D., Mogollón, J.M., Strasser, M., Pape, T., Bohrmann, G., Fekete, N., Spiess, V., Kasten, S., 2013. Subduction zone earthquake as potential trigger of submarine hydrocarbon seepage. Nat. Geosci. 6, 647-651.

Froelich, P.N., Klinkhammer, G.P., Bender, M.L., Luedtke, N.A., Heath, G.R., Cullen, D., Dauphin, P., Hammond, D., Hartman, B., Maynard, V., 1979. Early oxidation of organic matter in pelagic sediments of the eastern equatorial Atlantic: suboxic diagenesis. Geochim. Cosmochim. Acta 43, 1075-1090.

Greinert, J., Bohrmann, G., Suess, E., 2001. Gas hydrate-associated carbonates and methane venting at Hydrate Ridge: Classification, distribution and origin of carbonate lithologies. In Natural Gas Hydrates: Occurrence, Distribution and Detection (ed. Paull C. K. and Dillon W. P.), Vol. 124, pp. 99-113, American Geophysical Union.

Han, X., Suess, E., Liebetrau, V., Eisenhauer, A., Huang, Y, 2014. Past methane release events and environmental conditions at the upper continental slope of the South China

Sea: constraints by seep carbonates. Int. J. Earth Sci. DOI 10.1007/s00531-014-1018-5.

Haq, B.U., 1998. Natural gas hydrates: searching for the long-term climatic and slope-instability records. In Gas Hydrates: Relevance to World Margin stability and Climate Change (Eds. Henriet J.-P. and Mienert J.). Geol. Soc. Spec. Publ. 137, 303-318.

Hesselbo, S.P., Grocke, D.R., Jenkyns, H.C., Bjerrum, C.J., Farrimond, P., Morgans Bell, H.S., Green, O.R., 2000. Massive dissociation of gas hydrate during a Jurassic oceanic anoxic event. Nature 406, 392-395.

Hill, T.M., Kennett, J.P., Spero, H.J., 2004. High-resolution records of methane hydrate dissociation: ODP Site 893, Santa Barbara Basin. Earth Planet. Sci. Lett. 223, 127-140.

Hovland, M., Judd, A.G., 1988. Seabed pockmarks and seepages: Impact on Geology, Biology and Marine environment. Graham and Trotman (Eds.), London, Dordrecht, Boston, 293pp.

Hovland, M., Gardner, J.V., Judd, A.G., 2002. The significance of pockmarks to understand fluid flow processes and geohazards. Geofluids 2, 127-136.

Joye, S.M., Boetius, A., Orcutt, B.N., Montoya, J.P., Schulz, H.N., Erickson, M.J., Lugo, S.K., 2004. The anaerobic oxidation of methane and sulphate reduction in sediments from Gulf of Mexico cold seeps. Chem. Geol. 205, 219-238.

Judd, A.G., Hovland, M., Dimitrov, L.I., García Gil, S., Jukes, V., 2002. The geological methane budget at Continental Margins and its influence on climate change. Geofluids 2, 109–126.

Kennett, J.P., Cannariato, K.G., Hendy, I.L., Behl, R.J., 2000. Carbon isotopic evidence for methane hydrate instability during Quaternary interstadials. Science 288, 128-133.

Kutterolf, S., Liebetrau, V., Mörz, T., Freundt, A., Hammerich, T., Garbe-Schönberg, D., 2008. Lifetime and cyclicity of fluid venting at forearc mound structures determined by tephrostratigraphy and radiometric dating of authigenic carbonates. Geology 36, 707–710.

Kvenvolden, K.A., Lorenson, T.D., 2001. The Global Occurrence of Natural Gas Hydrates. In Natural Gas Hydrates: Occurrence, Distribution and Detection (ed. Paull C. K. and Dillon W. P.), Vol. 124, pp. 3-18, American Geophysical Union.

Lalou, C., Fontugne, M., Lallemand, S.E., Lauriat-Rage, A., 1992. Calyptogena-cemented rocks and concretions from the eastern part of Nankai accretionary prism: Age and geochemistry of uranium. Earth Planet. Sci. Lett. 109, 419-429.

Li, C.-H., Zhao, Q., Xu, H.-J., Feng, K., Liu, X.-W., 2014. Relation between relative permeability and hydrate saturation in Shenhu area, South China Sea. Appl. Geophys. 11, 207-214.

Liebetrau, V., Eisenhauer, A., Linke, P., 2010. Cold seep carbonates and associated coldwater corals at the Hikurangi Margin, New Zealand: new insights into fluid pathways, growth structures and geochronology. Mar. Geol. 272, 307–318.

Liebetrau, V., Augustin, N., Kutterolf, S., Schmidt, M., Eisenhauer, A., Garbe‑Schönberg, D., Weinrebe, W., 2014. Cold‑seep‑driven carbonate deposits at the Central American forearc: contrasting evolution and timing in escarpment and mound settings. Int. J. Earth Sci., DOI 10.1007/s00531-014-1045-2.

Loncke, L., Mascle, J., Fanil Science Party, 2004. Mud volcanoes, gas chimneys pockmarks and ridges in the Nile deep-sea fan (Eastern Mediterranean): geophysical evidences. Mar. Pet. Geol. 21, 669–689.

Ludwig, K.R., 2008. Using Isoplot/Ex, Version 3.70, A geochronological toolkit for Microsoft Excel: Berkeley Geochronology Ctr. Spec. Pub. 4.

Luff, R. Wallmann, K., 2003. Fluid flow, methane fluxes, carbonate precipitation and biogeochemical turnover in gas hydrate-bearing sediments at Hydrate Ridge, Cascadia Margin: numerical modelling and mass balances, Geochim. Cosmochim. Acta 67, 3403–3421.

Luff, R., Greinert, J., Wallmann, K., Klaucke, I., Suess, E., 2005. Simulation of long-term feedbacks from authigenic carbonate crust formation at cold vent sites. Chem. Geol. 216, 157-174.

Ménot G., Bard, E. 2010. Geochemical evidence for a large methane release during the last deglaciation from Marmara Sea sediments. Geochim. Cosmochim. Acta 74, 1537-1550.

Mienert, J., Vanneste, M., Bünz, S., Handreassen, K., Haflidason, H., Sejrup, H.P., 2005. Ocean warming and gas hydrate stability on the mid-Norwegian margin at the Storegga Slide. Mar. Petrol. Geol. 22, 233-244.

Milkov, A.V., 2004. Global estimates of hydrate-bound gas in marine sediments: how much is really out there? Earth Sci. Rev. 66, 183-197.

Naehr, T.H., Rodriguez, N.M., Bohrmann, G., Paull, C.K., Botz, R., 2000. Methane-derived authigenic carbonates associated with gas hydrate decomposition and fluid venting above the Blake Ridge Diapir. Proc. ODP Sci. Res. 164, 286–300.

Niewöhner, C., Hensen, C., Kasten, S., Zabel, M., Schulz, H.D., 1998. Deep sulphate reduction completely mediated by anaerobic methane oxidation in sediments of the upwelling area off Namibia. Geochim. Cosmochim. Acta 62, 455-464.

Nisbet, E., 1990. Climate change and methane. Nature 347, 23.

Panieri, G., James, R.H., Camerlenghi, A., Westbrook, G.K., Consolaro, C., Cacho, I., Cesari, V., Cervera, C.S., 2014. Record of methane emissions from the West Svalbard continental margin during the last 23.500 yrs revealed by δ13C of benthic foraminifera. Glob. Planet. Change 122, 151-160.

Pastouret, L., Chamley, H., Delibrias, G., Duplessy, J.-C., Thiede, J., 1978. Late Quaternary climatic changes in western tropical Africa deduced from dee-sea sedimentation off the Niger Delta. Oceanol. Acta 1, 217-232.

Pau, M., Hammer, O., 2013. Sediment mapping and long-term monitoring of currents and sediment fluxes in pockmarks in the Oslofjord, Norway. Mar. Geol. 346, 262-273

Pau, M., Hammer, O., Chand, S., 2014. Constraints on the dynamics of pockmarks in the SW Barents Sea: Evidence from gravity coring and high-resolution, shallow seismic profiles. Mar. Geol. 355, 330-345.

Pierre, C., Rouchy, J.M., Gaudichet, A., 2000. Diagenesis in the gas hydrate sediments of the Blake Ridge. Mineralogy and stable isotope compositions of the carbonate and sulphide minerals. Proc. ODP Sci. Res. 164, 139-145.

Reeburgh, W.S., 1976. Methane consumption in Cariaco Trench waters and sediments. Earth Planet. Sci. Lett. 28, 337-344.

Robinson, L.F., Belshaw, N.S., Henderson, G.M., 2004. U and Th concentrations and isotope ratios in modern carbonates and waters from the Bahamas. Geochim. Cosmochim. Acta 68, 1777-1789.

Rongemaille, E., 2011. Application des terres rares et de la datation U/Th à l'étude des carbonates authigènes de suintements froids: Exemple du delta profond du Niger. PhD Thesis, Institut Universitaire Européen de la Mer, Université de Bretagne Occidentale, Brest, 221 pp.

Rongemaille, E., Bayon, G., Pierre, C., Bollinger, C., Chu, N.C., Fouquet, Y., Riboulot, V., Voisset, M., 2011. Rare earth elements in cold seep carbonates from the Niger delta. Chem. Geol. 286, 196-206.

Ruffine, L., Caprais, J.-C., Bayon, G., Riboulot, V., Donval, J.-P., Etoubleau, J., Birot, D., Pignet, P., Rongemaille, E., Chazallon, B., Grimaud, S., Adamy, J., Charlou, J.-L., Voisset, M., 2013. Investigation of the geochemical dynamics of a hydrate-bearing pockmark in the Niger Delta. Mar. Petrol. Geol. 43, 297-309.

Smith, L.M., Sachs, J.P., Jennings, A.E., Anderson, D.M., de Vernal, A., 2001. Light δ^{13}C events during deglaciation of the East Greenland continental shelf attributed to methane release from gas hydrates. Geophys. Res. Lett. 28, 2217-2220.

Sowers, T., 2006. Late Quaternary atmospheric CH_4 isotope records suggests marine clathrates are stable. Nature 311, 838-840.

Stuiver, M., Reimer, P.J., Reimer, R.W., 2013. CALIB 7.0. [WWW program and documentation].

Suess, E., 2014. Marine cold seeps and their manifestations: geological control, biogeochemical criteria and environmental conditions. Int. J. Earth Sci., DOI 10.1007/s00531-014-1010-0

Sultan, N., Voisset, M., Marsset, T., Cauquil, E., Colliat, J.-L., Curinier, V., 2007. In situ detection of gas and gas hydrates using 3D seismic data and core penetration testing : Example from the Nigerian continental slope. Mar. Geol. 240, 235-255.

Sultan, N., Marsset, B., Ker, S., Marsset, T., Voisset, M., Vernant, A.M., Bayon, G., Cauquil, E., Adamy, J., Colliat, J.L., Drapeau, D., 2010. Hydrate dissolution as a potential mechanism for pockmark formation in the Niger delta. J. Geophys. Res 115, B08101.

Sultan, N., Bohrmann, G., Ruffine, L., Pape, T., Riboulot, V., Colliat, J.-L., De Prunelé, A., Dennielou, B., Garziglia, S., Himmler, T., Marsset, T., Peters, C.A., Rabiu, A., Wei, J., 2014. Pockmark formation and evolution in deep water Nigeria: Rapid hydrate growth versus slow hydrate dissolution. J. Geophys. Res.: Sol. Earth 119, 2679-2694.

Teichert, B.M.A., Eisenhauer, A., Bohrmann, G., Haase-Schramm, A., Bock, B., Linke, P., 2003. U/Th systematics and ages of authigenic carbonates from Hydrate Ridge, Cascadia Margin: recorders of fluid flow variations. Geochim. Cosmochim. Acta 67, 3845-3857.

Tong, H., Feng, D., Cheng, H., Yang, S., Wang, H., Min, A.G., Edwards, R.L., Chen, Z., Chen, D., 2013. Authigenic carbonates from seeps on the northern continental slope of the South China Sea: New insights into fluid sources and geochronology. Mar. Petrol. Geol. 43, 260-271.

Tréhu, A.M., et al., 2004. Three-dimensional distribution of gas hydrate beneath southern Hydrate Ridge: constraints from ODP Leg 204. Earth Planet. Sci. Lett. 222, 845-862.

Wallmann, K., Drews, M., Aloisi, G., Bohrmann, G., 2006. Methane discharge into the Black Sea and the global ocean via fluid flow through submarine mud volcanoes. Earth Planet. Sci. Lett. 248, 544-559.

Wallmann, K., Pinero, E., Burwicz, E., Haeckel, M., Hensen, C., Dale, A., Ruepke, L., 2012. The global inventory of methane hydrate in marine sediments: A theoretical approach. Energies 5, 2449-2498.

Watanabe, Y., Nakai, S., Hiruta, A., Matsumoto, R., Yoshida, K., 2008. U–Th dating of carbonate nodules from methane seeps off Joetsu, Eastern Margin of Japan Sea. Earth Planet. Sci. Lett. 272, 89–96.

Wei, J.-G. et al. (2015) Gas hydrate distributions in sediments of pockmarks from the Nigerian Margin - Results and interpretation from shallow drilling. Mar. Petrol. Geol. 59, 359-370.

Wirsig, C., Kowsmann, R.O., Miller, D.J., de Oliveira Godoy, J.M., Mangini, A., 2012. U/Th-dating and post-depositional alteration of a cold seep carbonate chimney from the Campos Basin offshore Brazil. Mar. Geol. 329-331, 24-33.

Zabel, M., Schneider, R.R., Wagner, T., Adegbie, A.T., de Vries, U., Kolonic, S., 2001. Late Quaternary climate changes in central Africa as inferred from terrigeneous input to the Niger Fan. Quat. Res. 56, 207-217.

Figure Captions

Figure 1: Bathymetric map of the studied area with position of the studied cores. This area corresponds to the collapsed summit of an anticline, which is delimited by two deep-rooted normal faults. Note that core N1-KSF-39 is located about 3 km south-west of core N2-KS-44.

Figure 2: Lithological description of core N2-KS-44 and corresponding pore-water sulphate, calcium and chloride profiles. Analytical uncertainties are within the size of the symbols. Note that original photographs of the studied carbonate concretions can be found in Bayon et al. (2007).

Figure 3: Downcore profiles of Al/Ti ratios for GeoB4901-8 (Zabel et al., 2001), N1-KSF-39 and N2-KS-44 (this study), and corresponding age control points. The chronology for core N1-KSF-39 relies on nine 14C-AMS radiocarbon analyses of mixed planktonic foraminifera fractions (Table 1), and tuning of its Al/Ti profile to the Al/Ti curve of core GeoB4901-8 (dashed lines); a well-dated sediment record also recovered in the Niger Delta deep province (Zabel et al., 2001). The age model for core N2-KS-44 was established by tuning its downcore Al/Ti profile to the nearby reference core N1-KSF-39 (dashed lines).

Figure 4: Backscatter electron (BSE) images of polished sections of carbonate-cemented breccias. (a,b) N2-KS-44_30 cm. (c,d) N2-KS-44_160 cm-1. (e) N2-KS-44_160 cm -2. HMg: microcrystalline high-Mg calcite-cemented mudstones; Fib: Radial fibrous crystals of aragonite; Btr: Botryoidal aragonite; Pyr: Framboidal pyrite; Bio: shell fragments (e.g. bivalves, foraminifera).

Figure 5: Backscatter electron (BSE) image and electron microprobe chemical maps for a carbonate-cemented breccia (N2-KS-44_75cm). HMg: microcrystalline high-Mg

calcite-cemented mudstones; Fib: Radial fibrous crystals of aragonite; Btr: Botryoidal aragonite; Bio: shell fragments.

Figure 6. Osmond isochron diagram for carbonate concretions and sediments at Site C (core N2-KS-44). Isochron ages are calculated from the slope of the isochrons. The sediment end-member (defined in Fig. 6) is used in all isochrons. The sediment associated with authigenic carbonates at 30 cm is also used in the isochron. Analytical errors are within the size of symbols.

Figure 7: Relationship between the depth of the sulphate-methane transition zone (SMTZ) and the depth of occurrence of gas hydrate nodules in the study area. The plot was constructed using data for core N2-KS-44 (this study) and previously published data (Rongemaille, 2011; Ruffine et al., 2013; Sultan et al., 2014; de Prunelé et al., 2015).

Figure 8: Al/Ti, weight proportion of aragonite (Bayon et al., 2007), sediment accumulation rates, and methane-derived carbonate U-Th ages *versus* stratigraphic age of sediment core N2-KS-44. The grey band represents the aragonite-rich layer between 30cm and 180 cm depth, which corresponds stratigraphically to the time interval 13.0 – 2.5 ka. The dashed black line represents the isochrone connecting carbonate and sediment samples that have the same age. Note that carbonate concretions below 160 cm depth are characterized by carbonate U-Th ages younger than corresponding stratigraphic ages, while carbonate-cemented breccias from the upper sediment layer display carbonate U-Th ages similar or older than stratigraphic ages.

Figure 9: (a to d) Conceptual model for gas hydrate dynamics and pockmark evolution at the studied site (see text for details).
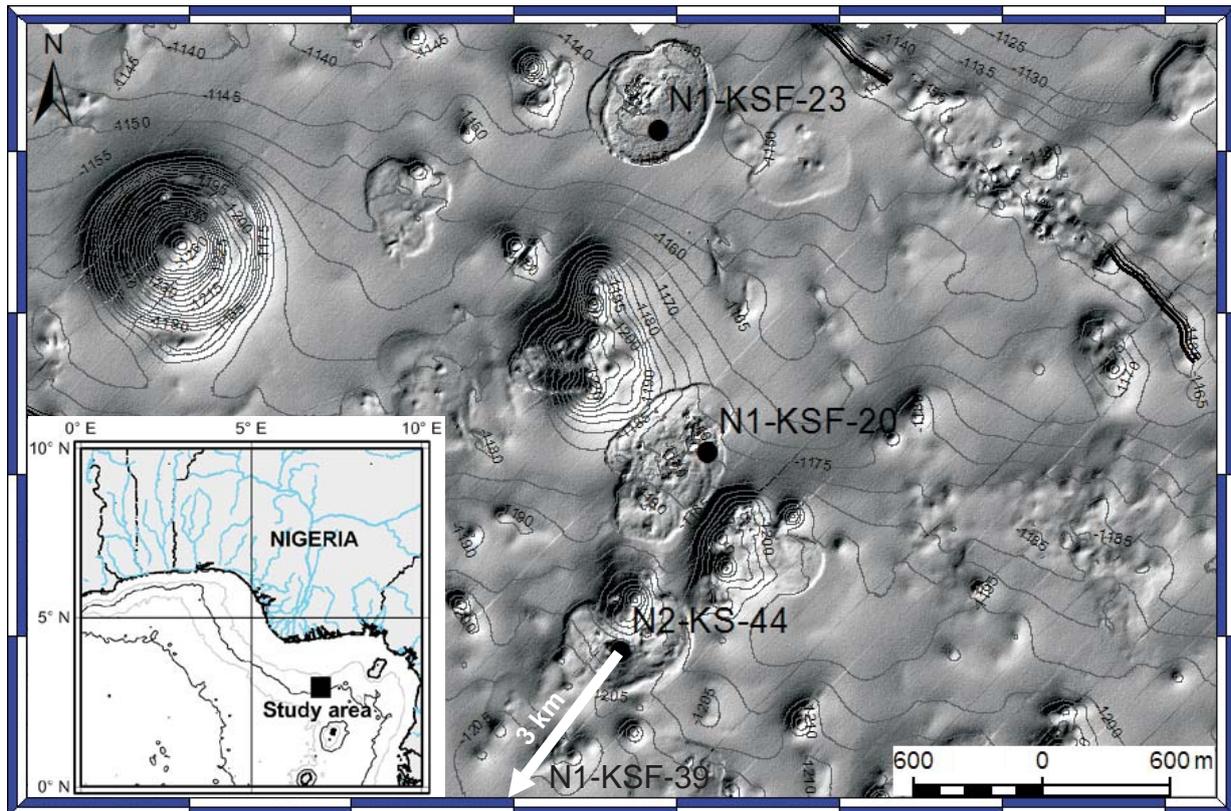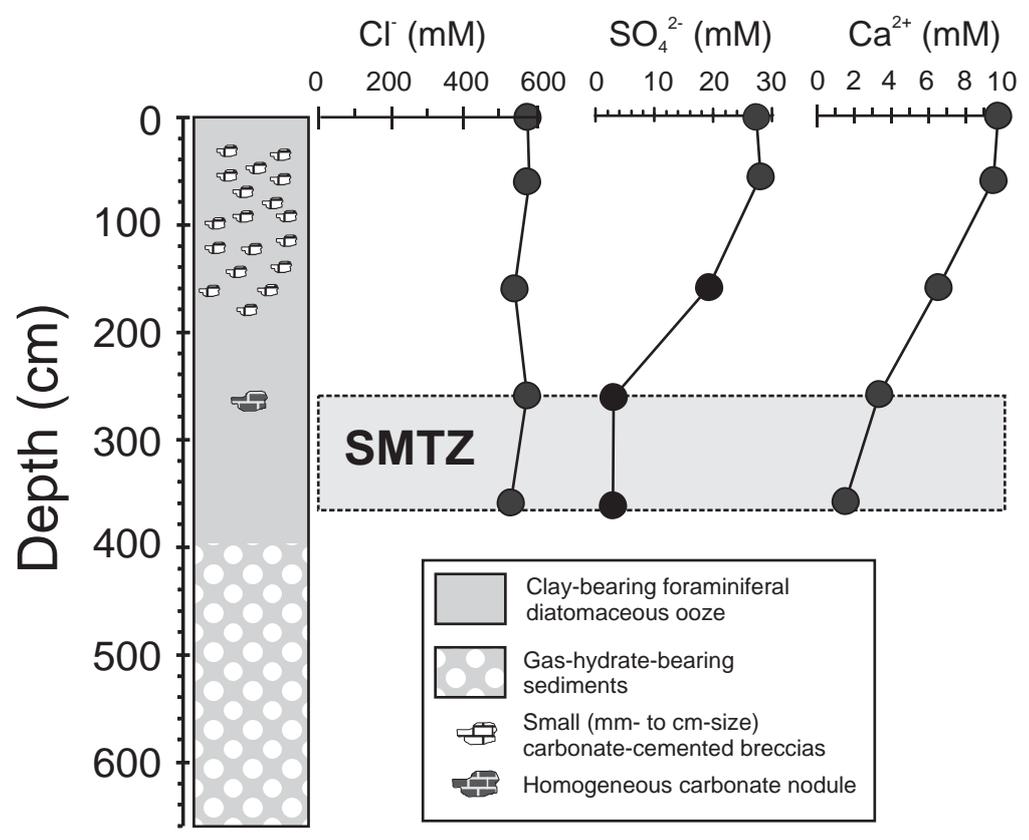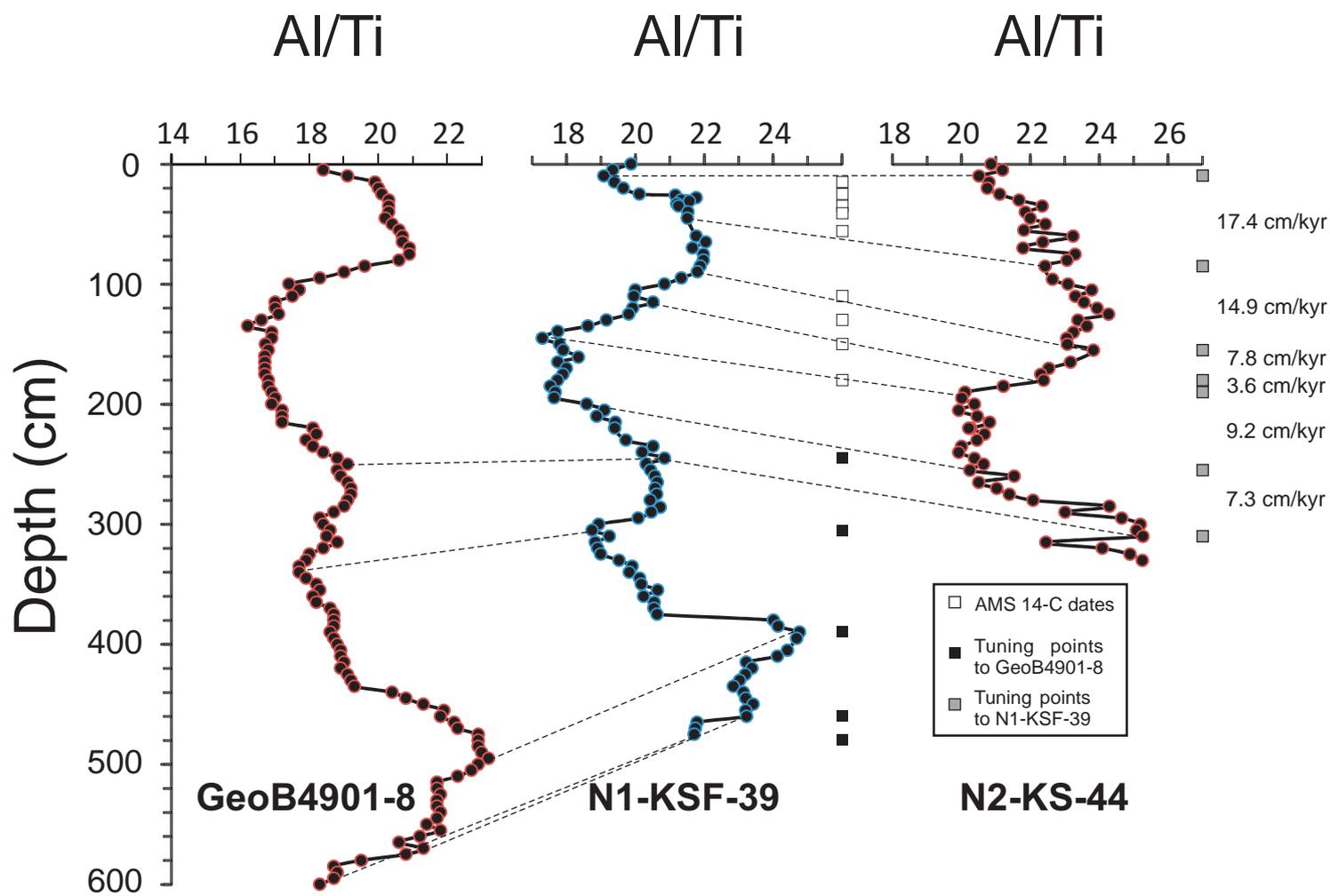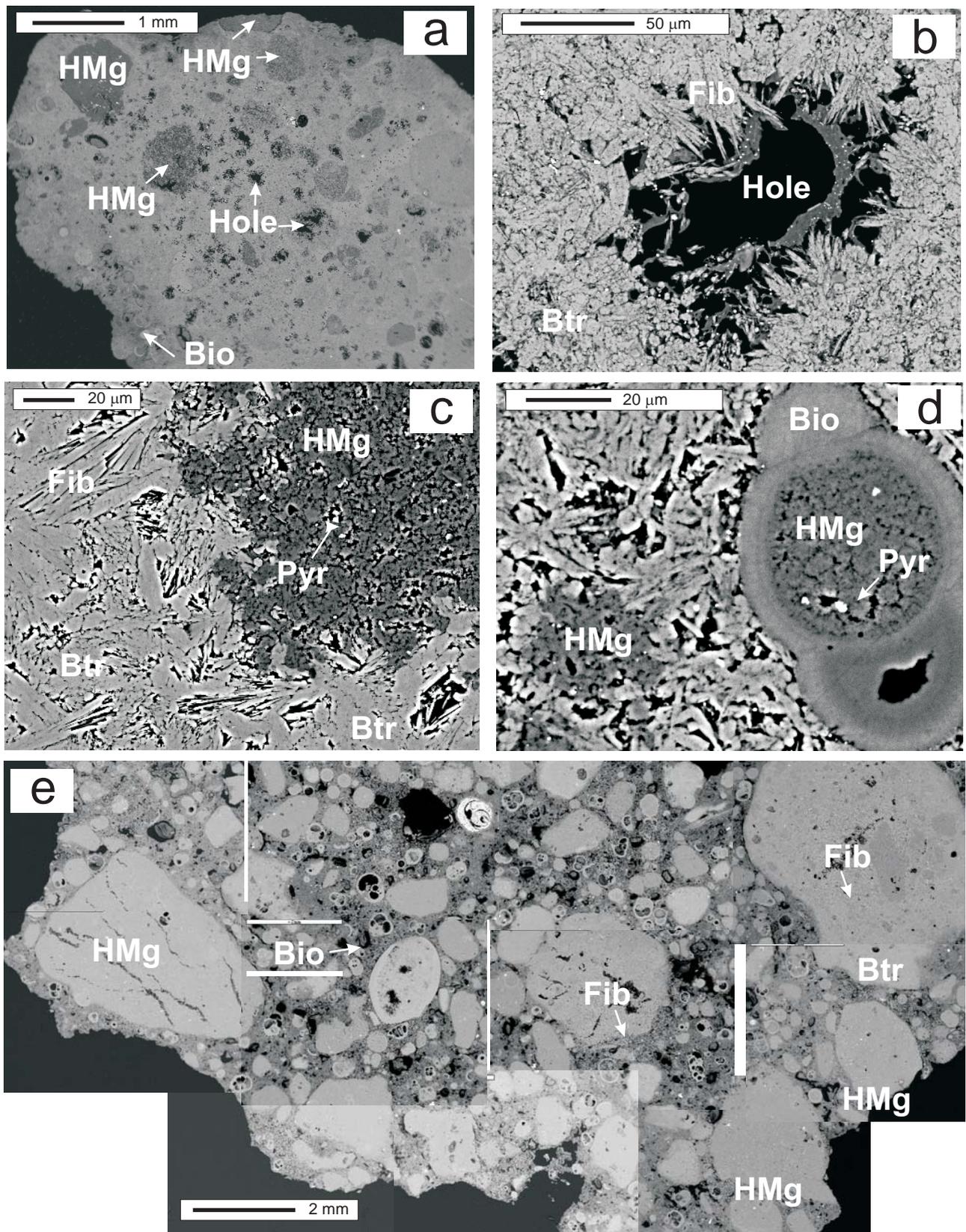
Figure1

Fig. 1

Figure2

Fig. 2

Figure3

Fig. 3

Figure4

Fig. 4

Figure5

Fig. 5

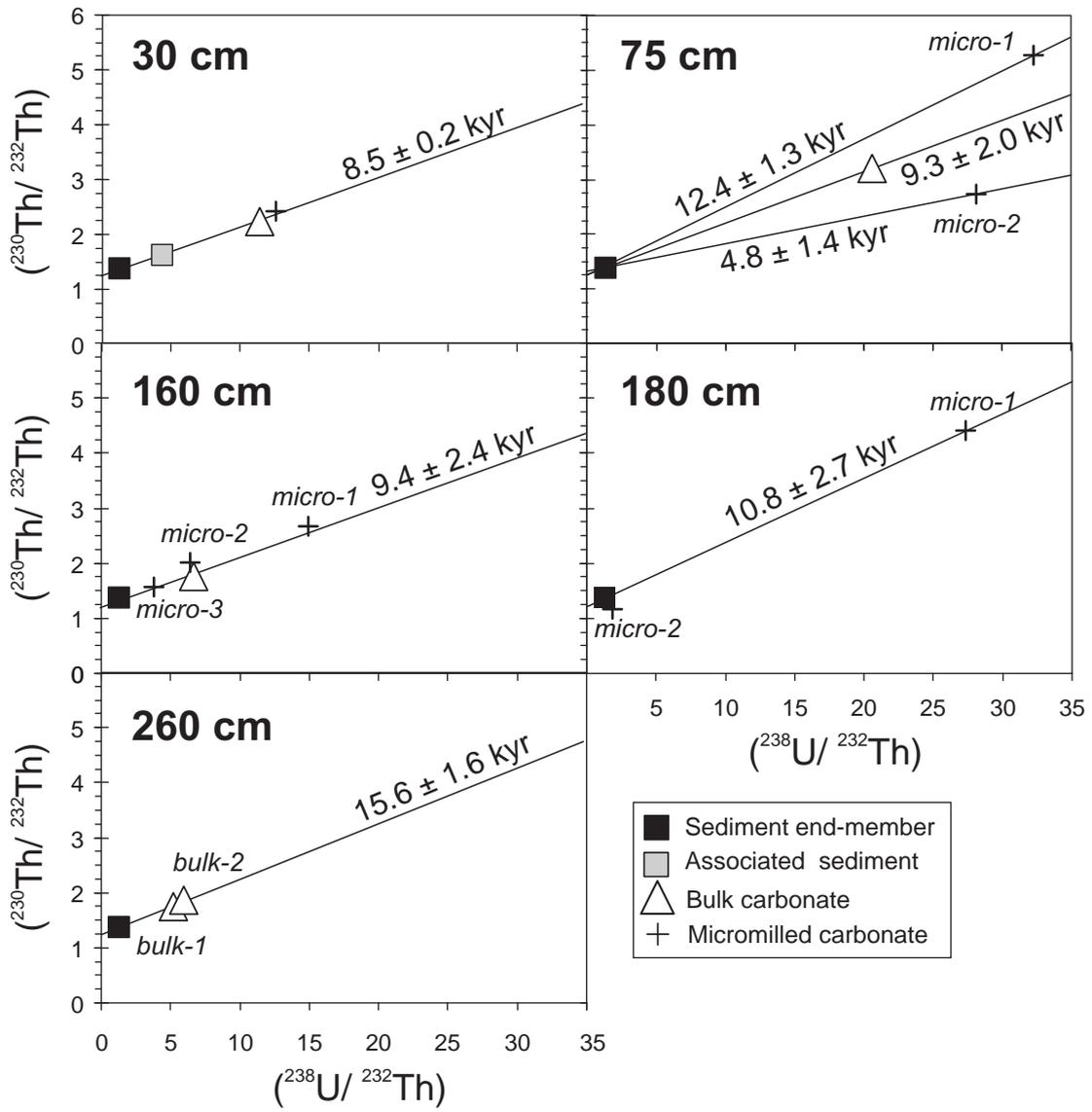**Figure6**
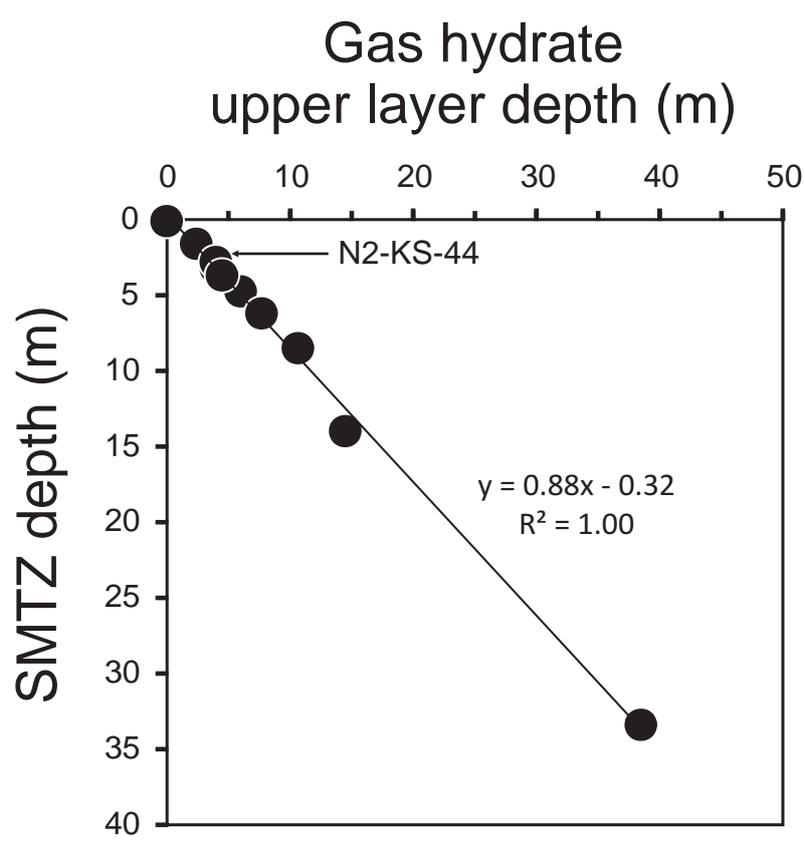

Fig. 6

Figure7

Fig. 7

Figure8

Fig. 8
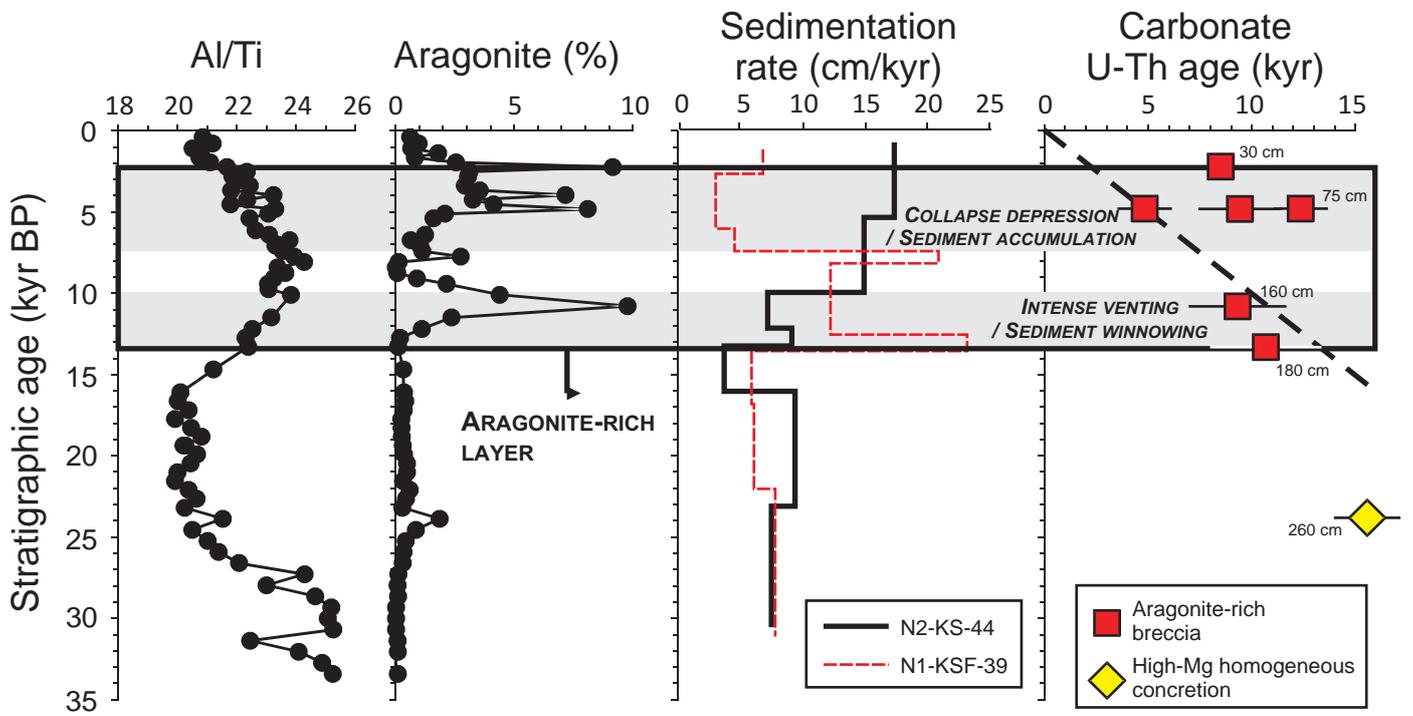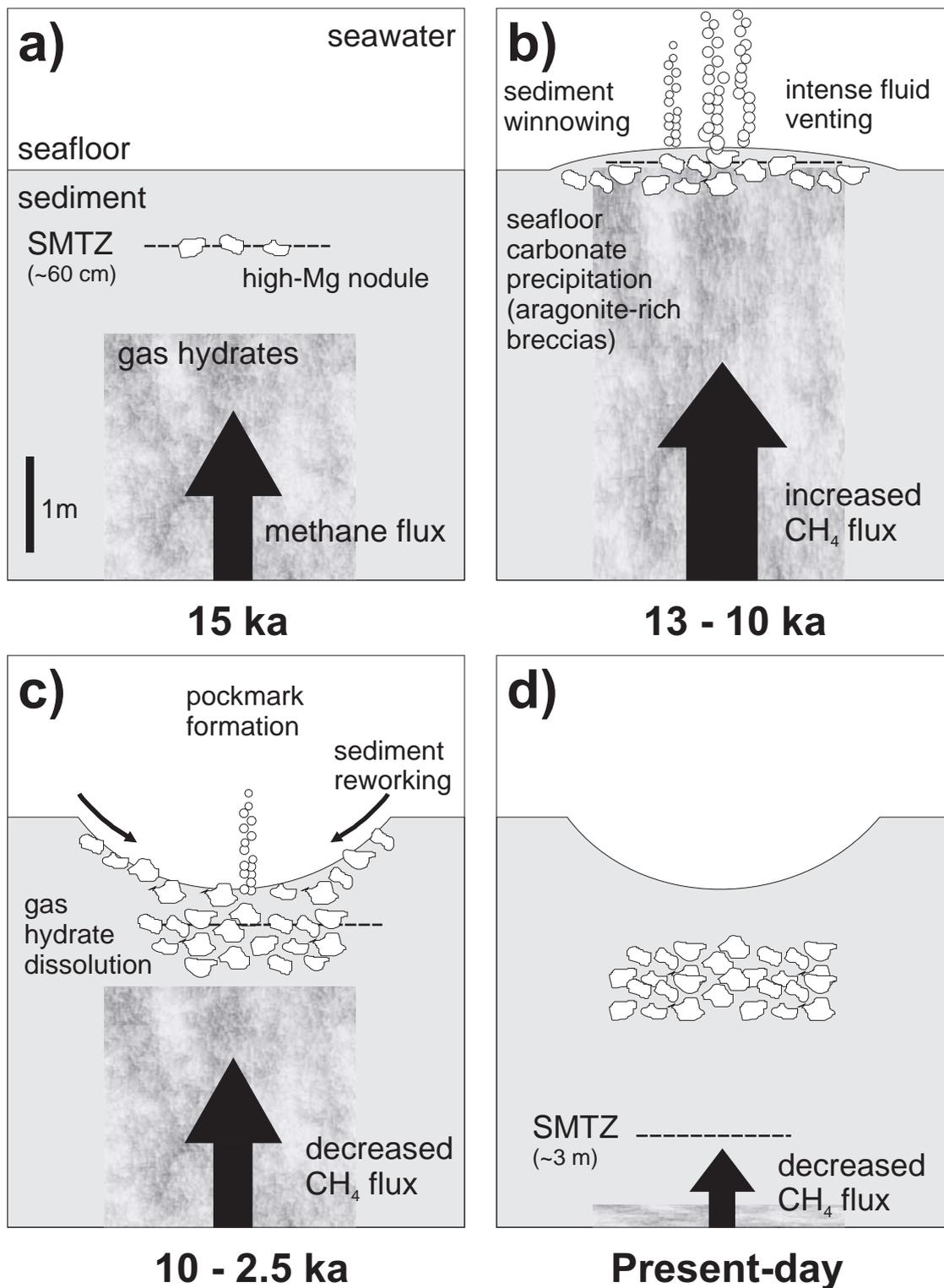
Figure9
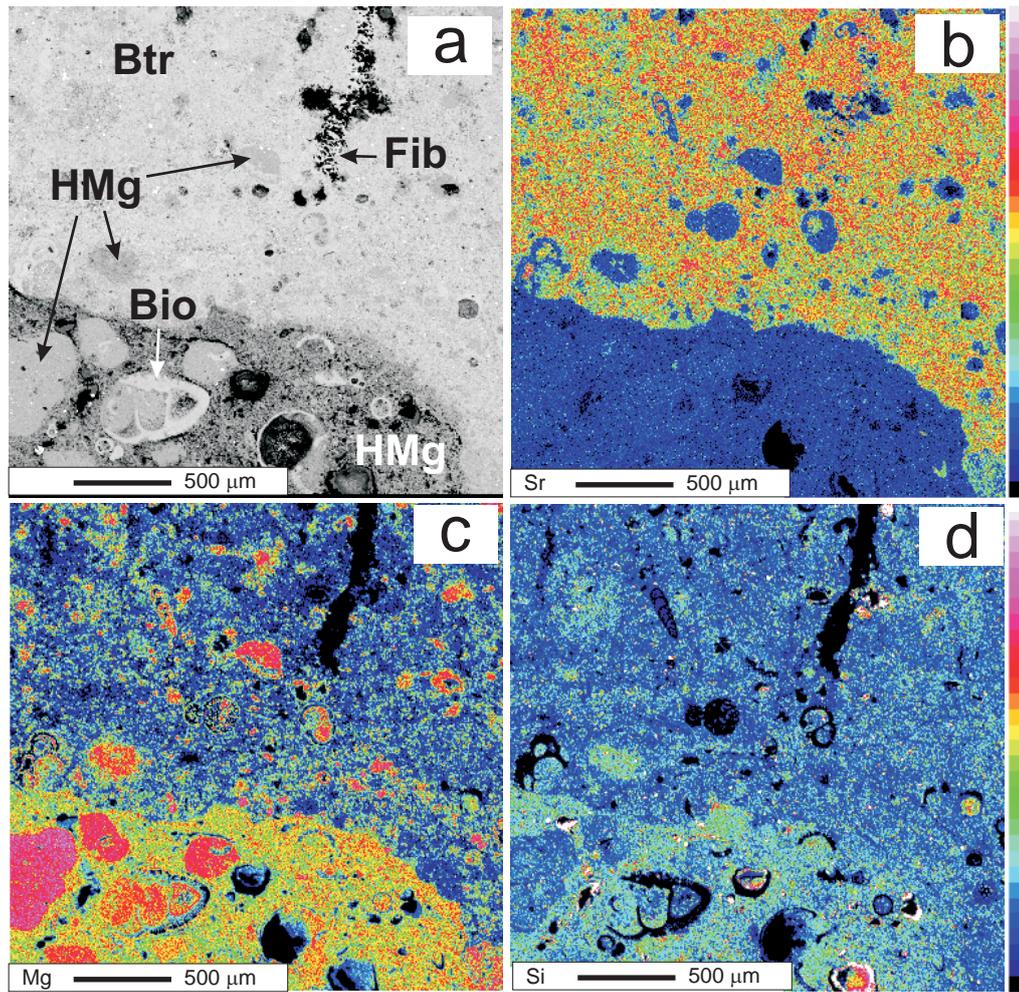
Fig. 9

Table 1. Radiocarbon dates (mixed planktonic foraminifera) and age control points for core N1-KSF-39

Core depth (cm)	Lab code	^{14}C age (yr BP)	Error (^{14}C age BP)	Cal. age range (1 σ) (yr BP)	Cal. age (yr BP)	Sedimentation rates (cm/kyr)
15	Poz-30684	2,115	30	1,599 - 1,800	1,698	6.5
25	Poz-20113	3,375	30	3,146 - 3,347	3,243	3.0
35	Poz-30686	6,100	40	6,418 - 6,633	6,527	4.7
41	Poz-20114	7,350	40	7,709 - 7,917	7,815	20.1
56	Poz-30687	8,100	50	8,419 - 8,711	8,560	12.2
110	Poz-20115	11,500	50	12,802 - 13,122	12,977	20.9
130	Poz-30689	12,450	60	13,772 - 14,095	13,932	5.7
150	Poz-30690	14,740	70	17,205 - 17,681	17,468	6.1
180	Poz-30691	18,880	100	22,022 - 22,550	22,352	7.8
245	Tuning to GeoB4901-8 (Zabel et al., 2001)				30,700	7.4
305	'				42,000	5.3
390	'				61,600	4.3
460	'				69,000	9.5
480	'				73,000	5.0

Table2
Click here to download Table: Table2.pdf

Table 2. Measured U-Th data (± 2s) for authigenic carbonates and sediments

Sample	Description	Weight (mg)	Dominant mineral	^{238}U (ppm)	^{230}Th (ppt)	$(^{230}Th/^{232}Th)$	$(^{238}U/^{232}Th)$	$\delta^{234}U_{(0)}$ (‰)
Sediments								
N2-KS-44_0 cm		50.1		7.35 ± 0.01	95.6 ± 0.6	1.380 ± 0.005	1.739 ± 0.008	135 ± 2
N2-KS-44_30 cm		49.7		16.52 ± 0.02	100.1 ± 0.6	1.627 ± 0.007	4.384 ± 0.018	141 ± 2
N2-KS-44_75 cm		50.0		12.34 ± 0.02	85.2 ± 0.4	1.300 ± 0.004	3.082 ± 0.014	133 ± 2
N2-KS-44_330 cm		49.8		5.54 ± 0.01	102.9 ± 0.6	1.326 ± 0.008	1.166 ± 0.004	104 ± 2
N1-KSF-20_248 cm		51.7		5.67 ± 0.01	80.9 ± 0.5	1.444 ± 0.007	1.654 ± 0.005	128 ± 2
N1-KSF-20_416 cm		52.5		5.28 ± 0.01	104.7 ± 0.7	1.516 ± 0.007	1.255 ± 0.004	114 ± 2
N1-KSF-23_0 cm		51.2		6.50 ± 0.01	97.7 ± 0.5	1.385 ± 0.006	1.507 ± 0.005	129 ± 2
N1-KSF-23_155 cm		52.5		8.88 ± 0.01	102.3 ± 0.5	1.262 ± 0.004	1.788 ± 0.006	95 ± 2
Carbonate-cemented breccias								
N2-KS-44_30 cm	bulk	41.1	Aragonite	11.47 ± 0.01	34.5 ± 0.1	2.20 ± 0.01	11.94 ± 0.03	144 ± 2
'	micromilled-1	1.00	Aragonite	8.88 ± 0.18	27.2 ± 1.0	2.42 ± 0.08	12.59 ± 0.37	144 ± 4
N2-KS-44_75 cm	bulk	109.9	Aragonite	22.46 ± 0.03	54.0 ± 0.2	3.30 ± 0.01	22.46 ± 0.07	149 ± 2
'	micromilled-1	1.09	Aragonite	23.52 ± 0.44	62.4 ± 1.5	5.28 ± 0.07	32.26 ± 0.85	156 ± 4
'	micromilled-2	1.19	HMg	21.56 ± 0.37	33.8 ± 0.9	2.74 ± 0.06	28.16 ± 0.68	140 ± 8
N2-KS-44_160 cm	bulk	50.3	Aragonite / HMg	7.13 ± 0.01	29.5 ± 0.2	1.72 ± 0.01	6.83 ± 0.03	133 ± 2
'	micromilled-1	1.15	Aragonite	9.04 ± 0.16	25.9 ± 0.8	2.67 ± 0.06	14.90 ± 0.37	133 ± 8
'	micromilled-2	1.29	Aragonite	5.92 ± 0.10	29.9 ± 0.8	2.01 ± 0.04	6.39 ± 0.15	130 ± 8
'	micromilled-3	1.10	HMg	4.77 ± 0.09	31.3 ± 0.7	1.57 ± 0.02	3.83 ± 0.10	124 ± 8
N2-KS-44_180 cm	micromilled-1	0.91	Aragonite	2.28 ± 0.06	5.2 ± 0.3	4.41 ± 0.22	27.35 ± 0.90	126 ± 8
'	micromilled-2	0.91	HMg	1.83 ± 0.04	17.7 ± 0.5	1.16 ± 0.02	1.87 ± 0.06	98 ± 8
Homogeneous carbonate nodule								
N2-KS-44_260 cm	bulk-1	104.2	HMg	4.44 ± 0.01	24.5 ± 0.1	1.76 ± 0.01	5.21 ± 0.01	127 ± 2
'	bulk-2	116.8	HMg	9.68 ± 0.01	49.9 ± 0.2	1.87 ± 0.01	5.94 ± 0.01	129 ± 2

Table3
Click here to download Table: Table3.pdf

Table 3. Activity ratios used for age calculation and isochron U-Th ages

Sample	Description	Dominant mineral	(^{232}Th/^{238}U)	(^{230}Th/^{238}U)	(^{234}U/^{238}U)	Two-point isochron age (kyr ± 2s)	Pseudo-isochron age (kyr ± 2s)	δ^{234}U (T) (‰)
Sediment end-member (±1s)								
			0.676 ± 0.124	0.939 ± 0.196	1.117 ± 0.016			
Carbonate-cemented breccias (±2s)								
N2-KS-44_30 cm	sediment		0.228 ± 0.001	0.370 ± 0.002	1.141 ± 0.002	n.d.		
'	bulk	Ara	0.087 ± 0.000	0.195 ± 0.001	1.144 ± 0.002	8.3 ± 3.8	8.5 ± 0.2	150 ± 4
'	micromilled-1	Ara	0.079 ± 0.004	0.187 ± 0.010	1.144 ± 0.005	8.6 ± 3.7		
N2-KS-44_75 cm	bulk	Ara	0.049 ± 0.000	0.155 ± 0.001	1.149 ± 0.002	9.3 ± 2.0	9.3 ± 2.0	155 ± 4
'	micromilled-1	Ara	0.031 ± 0.001	0.162 ± 0.004	1.156 ± 0.005	12.4 ± 1.3	12.4 ± 1.3	164 ± 5
'	micromilled-2	HMg	0.036 ± 0.001	0.096 ± 0.003	1.140 ± 0.009	4.8 ± 1.4	4.8 ± 1.4	143 ± 10
'	sediment		0.325 ± 0.001	0.422 ± 0.002	1.133 ± 0.002	n.d.		
N2-KS-44_160 cm	bulk	Ara/HMg	0.150 ± 0.001	0.265 ± 0.001	1.133 ± 0.002	7 ± 8		
'	micromilled-1	Ara	0.067 ± 0.001	0.175 ± 0.005	1.133 ± 0.009	9.0 ± 2.8	9.4 ± 2.4	141 ± 21
'	micromilled-2	Ara	0.156 ± 0.003	0.309 ± 0.009	1.130 ± 0.009	12 ± 8		
'	micromilled-3	HMg	0.261 ± 0.007	0.401 ± 0.013	1.124 ± 0.009	n.d.		
N2-KS-44_180 cm	micromilled-1	Ara	0.037 ± 0.001	0.140 ± 0.008	1.126 ± 0.009	9.5 ± 1.7	10.8 ± 2.7	129 ± 56
'	micromilled-2	HMg	0.534 ± 0.029	0.590 ± 0.033	1.098 ± 0.009	n.d.		
Homogeneous carbonate nodule (±2s)								
N2-KS-44_260 cm	bulk-1	HMg	0.192 ± 0.000	0.337 ± 0.002	1.127 ± 0.002	11 ± 10	15.6 ± 1.6	138 ± 6
'	bulk-2	HMg	0.168 ± 0.000	0.315 ± 0.001	1.129 ± 0.002	11 ± 9		

Supplementary Materials